

# Theory of the algebraic vortex liquid in an anisotropic spin- $\frac{1}{2}$ triangular antiferromagnet

Jason Alicea,<sup>1</sup> Olexei I. Motrunich,<sup>2</sup> and Matthew P. A. Fisher<sup>2</sup>

<sup>1</sup>*Physics Department, University of California, Santa Barbara, California 93106, USA*

<sup>2</sup>*Kavli Institute for Theoretical Physics, University of California, Santa Barbara, California 93106, USA*

(Received 18 December 2005; published 24 May 2006)

We explore spin- $\frac{1}{2}$  triangular antiferromagnets with both easy-plane and lattice exchange anisotropies by employing a dual vortex mapping followed by a fermionization of the vortices. Over a broad range of exchange anisotropy, this approach leads naturally to a “critical” spin liquid—the algebraic vortex liquid—which appears to be distinct from other known spin liquids. We present a detailed characterization of this state, which is described in terms of noncompact QED3 with an emergent SU(4) symmetry. Descendant phases of the algebraic vortex liquid are also explored, which include the Kalmeyer-Laughlin spin liquid, a variety of magnetically ordered states such as the well-known coplanar spiral state, and supersolids. In the range of exchange anisotropy where the “square lattice” Néel ground state arises, we demonstrate that anomalous “roton” minima in the excitation spectrum recently reported in series expansions can be accounted for within our approach.

DOI: [10.1103/PhysRevB.73.174430](https://doi.org/10.1103/PhysRevB.73.174430)

PACS number(s): 75.10.Jm, 75.40.Gb

## I. INTRODUCTION

A fundamental theoretical challenge in strongly correlated systems lies in understanding the behavior of frustrated quantum magnets, whose properties often bear little resemblance to those of their classical counterparts. In the most exotic scenario, quantum fluctuations are sufficiently strong to disorder the system even at zero temperature, and a spin liquid ground state emerges. Historically, Anderson originally suggested that the spin- $\frac{1}{2}$  Heisenberg triangular antiferromagnet may realize such a quantum-disordered ground state.<sup>1</sup> It is now recognized that with only nearest-neighbor exchange the true ground state on the triangular lattice is the magnetically ordered  $\sqrt{3} \times \sqrt{3}$  phase, though the order is significantly diminished relative to the classical state.<sup>2,3</sup> It is conceivable, then, that a spin liquid may arise with not too drastic perturbations to the model, and the triangular lattice has thus remained a prominent setting in the search for two-dimensional spin liquids.

Recent experiments on the spin- $\frac{1}{2}$  anisotropic triangular antiferromagnet Cs<sub>2</sub>CuCl<sub>4</sub> stimulated renewed interest in possible spin-liquid phases proximate to the nearest-neighbor Heisenberg model.<sup>4,5</sup> This material is accurately modeled by an anisotropic Heisenberg Hamiltonian supplemented by a weak Dzyaloshinskii-Moriya interaction.<sup>6</sup> Although long-range spiral order develops at temperatures  $T \lesssim 0.62$  K, the dynamical structure factor measured via neutron scattering exhibits “critical” power laws at intermediate energies, both in the ordered phase and in a range of temperatures above  $T_N$ . This unusual power-law behavior in the excitation spectrum is highly suggestive of spinon deconfinement that is characteristic of spin liquids.

A variety of theoretical approaches have been employed to capture spin liquids on the triangular lattice. Kalmeyer and Laughlin exploited a mapping between the spin- $\frac{1}{2}$  Heisenberg model and hard-core bosons in a magnetic field to obtain a “chiral” spin liquid which breaks time-reversal symmetry.<sup>7,8</sup> Their arguments were subsequently reformulated by Yang *et al.*,<sup>9</sup> who arrived at the chiral spin liquid by fermionizing the spins using Chern-Simons flux attachment<sup>10</sup>

and expanding around a “flux-smeared” mean-field state. Using a slave-boson representation of the spin operators, Sachdev explored an Sp( $N$ ) generalization of the Heisenberg model, and in the large- $N$  limit obtained a  $Z_2$  spin liquid ground state, which breaks no symmetries.<sup>11</sup> The  $Z_2$  spin liquid was later realized microscopically in a quantum dimer model on the triangular lattice.<sup>12</sup> Finally, a large class of spin liquids was studied by Zhou and Wen using a slave fermion representation of the spins.<sup>13</sup> Whereas excitations in both the chiral and  $Z_2$  spin liquids are gapped, the slave fermion mean-field approach can give rise to so-called “algebraic spin liquids,” which admit *gapless* spin excitations and power-law spin correlations.

In this paper we pursue an alternate approach to the spin- $\frac{1}{2}$  triangular antiferromagnet, and use vortex duality to attack the problem coming from the easy-plane regime. Duality has been a powerful tool for exploring unconventional phases such as valence bond solids and spin liquids in quantum spin systems,<sup>14–18</sup> as well as complex charge-ordered states in bosonic systems.<sup>19–24</sup> The main difficulty here is that vortices are at finite density, which is familiar from dual approaches to the fractional quantum Hall problem. As an initial step towards applying duality to frustrated spin systems, in Ref. 25 we examined integer-spin triangular antiferromagnets with easy-plane symmetry from the vortex perspective. By *fermionizing* the vortices using Chern-Simons flux attachment, it was shown that an effective low-energy dual formulation can be derived, which was argued to reproduce the physics of a more direct Landau-Ginzburg-Wilson analysis of the spin model. While this approach is reminiscent of the spin fermionization adopted by Yang *et al.*,<sup>9</sup> we emphasize that alternatively fermionizing vortices is advantageous because the vortices interact logarithmically, which allows for a more controllable treatment of Chern-Simons gauge fluctuations.

Here we extend the fermionized vortex approach to the spin- $\frac{1}{2}$  triangular antiferromagnet with easy-plane symmetry and anisotropic nearest-neighbor exchanges  $J$  and  $J'$  as shown in Fig. 1. This formalism allows us to explore the phase diagram of the spin model in a setting where a more

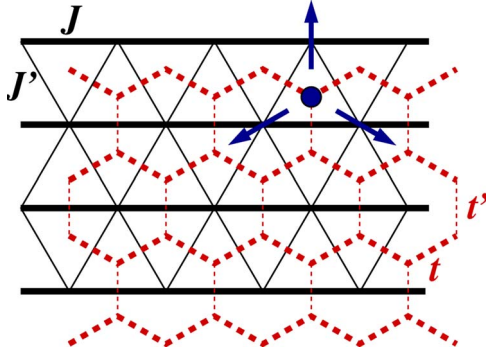


FIG. 1. (Color online) Triangular lattice and the dual honeycomb on which vortices reside. Spins shown illustrate a vortex. The spin exchange and vortex hopping amplitudes are generally anisotropic, with  $J'/J \sim t'/t$ .

conventional Landau analysis of the spin model is *not* accessible due to Berry phases. Remarkably, over a broad range of anisotropy  $J'/J \leq 1.4$  this approach leads naturally, with the simplest flux-smeared mean-field starting point, to a “critical” spin liquid that we will refer to as the algebraic vortex liquid. This state was introduced earlier and applied to  $\text{Cs}_2\text{CuCl}_4$  in a short letter, Ref. 26, and is characterized in detail here. Schematically, vortices form a critical state with four Dirac nodes, and interact via a fluctuating gauge field representing the original boson current fluctuations. Already on the mean-field level, the gapless character of the vortex state implies power-law  $S^z$  and  $S^\pm$  spin correlations at specific wave vectors shown in Figs. 6 and 7, respectively. Such momenta for low-energy excitations in the spin system are determined by short-distance physics in the frustrated magnet, and we propose that this physics is well captured in the vortex treatment.

Going beyond a mean-field analysis, we argue that the algebraic vortex liquid is described by QED3 with an emergent global  $\text{SU}(4)$  flavor symmetry, which has further implications for the dynamical spin correlations. In particular, as a consequence of the  $\text{SU}(4)$  symmetry the in-plane spin structure factor exhibits enhanced universal power-law correlations with the *same exponent* at several momenta in the Brillouin zone: the spiral ordering wave vectors  $\pm\mathbf{Q}$  and momenta  $\mathbf{K}_{1,2,3}$  at the midpoints of the Brillouin zone edges (see Fig. 7). The out-of-plane spin structure factor meanwhile has enhanced correlations only at the spiral ordering wave vectors  $\pm\mathbf{Q}$ . These nontrivial properties distinguish the algebraic vortex liquid from other known spin liquids. Interestingly, the prominence of momenta  $\mathbf{K}_{1,2,3}$  in the theory appears to be consistent with recent series expansion studies of the Heisenberg triangular antiferromagnet,<sup>27</sup> which observe excitation energies at these wave vectors which are dramatically reduced relative to linear spin-wave theory. Moreover, the prediction of “active” momenta  $\pm\mathbf{Q}$  and  $\mathbf{K}_{1,2}$  in the anisotropic system seems to capture the neutron scattering data for  $\text{Cs}_2\text{CuCl}_4$ .<sup>4,5</sup>

The phase diagram in the vicinity of the algebraic vortex liquid is also explored, and found to be rather rich. Nearby phases include the Kalmeyer-Laughlin chiral spin liquid, numerous magnetically ordered states including the coplanar

spiral state, and variants of supersolids discussed recently.<sup>28–31</sup>

In the range of anisotropy  $J'/J \geq 1.4$ , our treatment captures the “square-lattice” Néel ordered state, which is the expected ground state in this regime.<sup>32</sup> Here, we demonstrate in a particularly clear setting that anomalous “roton” minima in the excitation spectrum observed by series expansion studies can indeed be accounted for as low-energy vortex-antivortex excitations.<sup>27,32</sup> We further predict that these low-energy rotons may have still more dramatic effects in the easy-plane regime, which would be useful to explore using series expansions.

The paper is organized as follows. The spin model and the dual vortex mapping are introduced in Sec. II. In Sec. III the fermionized vortex theory is developed. We first discuss the “roton” excitations in the Néel phase arising when  $J'/J \geq 1.4$ . We then obtain a low-energy effective theory for  $J'/J \leq 1.4$  which contains a description of the algebraic vortex liquid. Section IV focuses on the properties of the algebraic vortex liquid, including its stability, symmetries, and dynamic spin correlations. The proximate phases of the algebraic vortex liquid are explored in Sec. V, and we conclude with a discussion in Sec. VI.

## II. MODEL

### A. Easy-plane spin model

We begin by considering an easy-plane, anisotropic spin- $\frac{1}{2}$  triangular antiferromagnet modeled by an XXZ Hamiltonian with nearest-neighbor exchange,

$$H_0 = \frac{1}{2} \sum_{\langle \mathbf{r}\mathbf{r}' \rangle} J_{\mathbf{r}\mathbf{r}'} (S_{\mathbf{r}}^+ S_{\mathbf{r}'}^- + \text{H.c.}) + \sum_{\langle \mathbf{r}\mathbf{r}' \rangle} J_{\mathbf{r}\mathbf{r}'}^z S_{\mathbf{r}}^z S_{\mathbf{r}'}^z, \quad (1)$$

where  $S_{\mathbf{r}}^\pm = S_{\mathbf{r}}^x \pm iS_{\mathbf{r}}^y$  are the usual spin raising and lowering operators. As illustrated in Fig. 1, we take the in-plane exchange energy to be  $J_{\mathbf{r}\mathbf{r}'} = J$  along bold horizontal links and  $J_{\mathbf{r}\mathbf{r}'} = J'$  along diagonal links of the triangular lattice. The out-of-plane exchange is defined to be  $J_{\mathbf{r}\mathbf{r}'}^z \equiv \gamma J_{\mathbf{r}\mathbf{r}'}$ , with  $0 < \gamma < 1$  to satisfy the easy-plane condition.

It is convenient to work with the easy-plane spin model recast in terms of quantum rotors by introducing an integer-valued boson number  $n_{\mathbf{r}}$  and its conjugate phase  $\varphi_{\mathbf{r}}$ . Upon identifying  $S_{\mathbf{r}}^z \rightarrow n_{\mathbf{r}} - 1/2$  and  $S_{\mathbf{r}}^\pm \rightarrow e^{i\varphi_{\mathbf{r}}}$ , the Hamiltonian reads

$$H_0 = \sum_{\langle \mathbf{r}\mathbf{r}' \rangle} J_{\mathbf{r}\mathbf{r}'} \cos(\varphi_{\mathbf{r}} - \varphi_{\mathbf{r}'}) + U \sum_{\mathbf{r}} (n_{\mathbf{r}} - 1/2)^2 + \sum_{\langle \mathbf{r}\mathbf{r}' \rangle} J_{\mathbf{r}\mathbf{r}'}^z (n_{\mathbf{r}} - 1/2)(n_{\mathbf{r}'} - 1/2). \quad (2)$$

The  $U$  term above energetically enforces the constraint of having either 0 or 1 boson per site as required for modeling a spin- $\frac{1}{2}$  system.

The XXZ Hamiltonian  $H_0$  respects a number of internal and discrete lattice symmetries which we now enumerate. The model exhibits  $U(1)$  spin symmetry and is invariant under time reversal  $\mathcal{T}$  and a “particle-hole” transformation  $\mathcal{C}$

which sends  $(S^x, S^y, S^z) \rightarrow (S^x, -S^y, -S^z)$ . Under these operations, the rotor fields transform as follows:

$$U(1): n \rightarrow n, \quad e^{i\varphi} \rightarrow e^{i(\varphi+\alpha)}, \quad (3)$$

$$C: n \rightarrow 1-n, \quad e^{i\varphi} \rightarrow e^{-i\varphi}, \quad (4)$$

$$\mathcal{T}: n \rightarrow 1-n, \quad e^{i\varphi} \rightarrow -e^{-i\varphi}, \quad (5)$$

where  $\alpha$  is a constant and  $\mathcal{T}$  is an antiunitary operation which sends  $i \rightarrow -i$ . The model also preserves translations  $T_{\delta\mathbf{r}}$  by triangular lattice vectors  $\delta\mathbf{r}$ , as well as  $x$ -reflections  $\mathcal{R}_x$  and inversions (i.e.,  $\pi$  rotations)  $R_\pi$  about a triangular lattice site. Rather than considering the  $x$ -reflections  $\mathcal{R}_x$ , it will be useful for subsequent developments to work with a modified antiunitary reflection  $\tilde{\mathcal{R}}_x \equiv \mathcal{R}_x \mathcal{C} \mathcal{T}$ . The latter operations transform the rotor fields as

$$\tilde{\mathcal{R}}_x: n_{\mathbf{r}} \rightarrow n_{\mathbf{r}'}, \quad e^{i\varphi_{\mathbf{r}}} \rightarrow -e^{i\varphi_{\mathbf{r}'}}, \quad (6)$$

where  $\mathbf{r}'$  is an appropriately reflected coordinate. In the isotropic limit  $J=J'$ , the XXZ Hamiltonian additionally preserves  $\pi/3$  rotations  $R_{\pi/3}$  about a triangular lattice site;  $R_\pi$  is then no longer an independent symmetry since  $R_{\pi/3}^3 = R_\pi$ .

In this paper we are interested in exploring the phase diagram accessible with the above XXZ spin model as a starting point. In particular, as the low spin and geometric frustration strongly suppress the tendency to magnetically order, it is natural to ask whether spin-liquid phases can be realized with not too drastic perturbations to the model. To this end, we would like to derive an effective theory that governs the low-energy behavior of the spin system. This is, for instance, readily achieved for the integer-spin analogue of Eq. (1), and the phase diagram can be explored within a standard Landau analysis. However, for the spin- $\frac{1}{2}$  system studied here a similar direct analysis of the spin model is hindered by the presence of Berry phases. Consequently, obtaining a low-energy theory is largely intractable in this formulation.

To proceed we utilize an alternative dual approach, introduced in the context of integer-spin systems in Ref. 25, wherein one considers a reformulation of the problem in terms of *fermionized vortices*. In this framework, the basic degrees of freedom one works with are vortices—topological defects in which the phases  $\varphi_{\mathbf{r}}$  of the spins wind by  $2\pi$  around a triangular plaquette as in Fig. 1—rather than the spins themselves. Although the vortices as defined are bosonic, it will prove extremely useful to fermionize them in a manner familiar from the fractional quantum Hall effect via Chern-Simons flux attachment. Doing so enables us to obtain a low-energy dual theory, which as we will demonstrate leads naturally to a “critical” spin-liquid phase, the algebraic vortex liquid.

## B. Dual vortex mapping

We proceed now to the dual vortex theory. We forgo the details of the duality mapping as these are provided in Sec. III of Ref. 25 in a very similar setting, and instead emphasize the important physical aspects of the dual theory. Implementing the duality transformation on the quantum rotor Hamil-

tonian Eq. (2),<sup>19</sup> one obtains a theory of bosonic vortices with “electromagnetic” interactions hopping among sites of the dual honeycomb lattice depicted by the dashed lines in Fig. 1. The vortices interact via a “vector potential”  $a_{\mathbf{x}\mathbf{x}'} \in \mathbb{R}$  and a conjugate “electric field”  $e_{\mathbf{x}\mathbf{x}'}$ , which reside on honeycomb links and mediate a logarithmic vortex repulsion. Here  $\mathbf{x}, \mathbf{x}'$  denote nearest-neighbor honeycomb sites. (Throughout, we distinguish sites of the honeycomb and triangular lattices by the labels “ $\mathbf{x}$ ” and “ $\mathbf{r}$ ,” respectively.) These dual gauge fields satisfy the commutation relation  $[e_{\mathbf{x}\mathbf{x}'}, a_{\mathbf{x}\mathbf{x}'}] = i$  and commute on different links. In-plane spin components are encoded in this formulation through the “electric field” and the vortices. The  $S^z$  component of spin meanwhile appears as a dual “magnetic flux,”

$$S_{\mathbf{r}}^z \sim \frac{1}{2\pi} (\Delta \times a)_{\mathbf{r}}, \quad (7)$$

where  $(\Delta \times a)_{\mathbf{r}}$  signifies a lattice curl of  $a_{\mathbf{x}\mathbf{x}'}$  around the hexagon encircling site  $\mathbf{r}$  of the triangular lattice. Although  $a_{\mathbf{x}\mathbf{x}'}$  roams over the real numbers, the desired half-integer values of  $S^z$  in Eq. (7) are imposed energetically in the dual theory.

In terms of a vortex number operator  $N_{\mathbf{x}}$  and vortex creation operator  $e^{i\theta_{\mathbf{x}}}$ , the dual vortex Hamiltonian can be expressed as

$$\mathcal{H}_{\text{dual}} = \mathcal{H}_a - \sum_{\langle \mathbf{x}\mathbf{x}' \rangle} 2t_{\mathbf{x}\mathbf{x}'} \cos(\theta_{\mathbf{x}} - \theta_{\mathbf{x}'} - a_{\mathbf{x}\mathbf{x}'} - a_{\mathbf{x}\mathbf{x}'}^0) \quad (8)$$

together with a Gauss’s law constraint for the “electric field,”

$$(\Delta \cdot e)_{\mathbf{x}} = N_{\mathbf{x}} - 1/2. \quad (9)$$

Here  $a_{\mathbf{x}\mathbf{x}'}^0$  is a static gauge field satisfying  $(\Delta \times a^0)_{\mathbf{r}} = \pi$ , and  $(\Delta \cdot e)_{\mathbf{x}}$  denotes a lattice divergence of  $e_{\mathbf{x}\mathbf{x}'}$  at site  $\mathbf{x}$ . Moreover,  $\mathcal{H}_a$  describes the gauge field dynamics,

$$\begin{aligned} \mathcal{H}_a = & \sum_{\langle \mathbf{x}\mathbf{x}' \rangle} \mathcal{J}_{\mathbf{x}\mathbf{x}'} e_{\mathbf{x}\mathbf{x}'}^2 + \mathcal{U} \sum_{\mathbf{r}} (\Delta \times a)_{\mathbf{r}}^2 \\ & + \sum_{\langle \mathbf{r}\mathbf{r}' \rangle} \mathcal{J}_{\mathbf{r}\mathbf{r}'} (\Delta \times a)_{\mathbf{r}} (\Delta \times a)_{\mathbf{r}'}, \end{aligned} \quad (10)$$

with  $\mathcal{U} = U/(2\pi)^2$ ,  $\mathcal{J}_{\mathbf{r}\mathbf{r}'} = J_{\mathbf{r}\mathbf{r}'}^z/(2\pi)^2$ , and  $\mathcal{J}_{\mathbf{x}\mathbf{x}'} = 2\pi^2 J'$  on the bold zigzag honeycomb links in Fig. 1 while  $\mathcal{J}_{\mathbf{x}\mathbf{x}'} = 2\pi^2 J$  on vertical honeycomb links.

The cosine term in Eq. (8) describes nearest-neighbor vortex hopping in an average background of  $\pi$  flux per hexagon. This background “magnetic flux” is provided by the static gauge field  $a_{\mathbf{x}\mathbf{x}'}^0$ , and arises because  $S^z$  is half-integer valued in the original spin model. (The average background flux for an integer spin system, in contrast, is trivial.<sup>25</sup>) The hopping amplitudes  $t_{\mathbf{x}\mathbf{x}'}$  are chosen to be anisotropic to reflect the spin exchange anisotropy. In particular, as illustrated in Fig. 1 we take  $t_{\mathbf{x}\mathbf{x}'} = t$  on the bold zigzag links of the honeycomb and  $t_{\mathbf{x}\mathbf{x}'} = t'$  on vertical links, with  $t'/t \sim J'/J$  since vortices hop more easily across weak spin links than strong spin links.

An important feature of the dual theory is that with our conventions<sup>25</sup> the bosonic vortices are at *half-filling*, which is a direct consequence of the underlying frustration in the spin model. For example, in the classical  $\sqrt{3} \times \sqrt{3}$  spin-ordered state we define the vortex number to be one on “up” triangles

TABLE I. Transformation properties of fields in the dual bosonic-vortex formulation under the discrete microscopic symmetries. The lattice coordinates, which also transform appropriately under the lattice symmetries, have been suppressed on all fields for brevity.

$T_{\partial\tau}, R_{\pi}, R_{\pi/3}$ (isotropic limit)	$\mathcal{C}$	$\tilde{\mathcal{R}}_{\mathbf{x}}, \mathcal{T}$
$a^0 \rightarrow a^0$	$a^0 \rightarrow -a^0$	$a^0 \rightarrow -a^0$
$a \rightarrow a$	$a \rightarrow -a$	$a \rightarrow -a$
$e \rightarrow e$	$e \rightarrow -e$	$e \rightarrow e$
$\theta \rightarrow \theta$	$\theta \rightarrow -\theta$	$\theta \rightarrow -\theta$
$N \rightarrow N$	$N \rightarrow 1-N$	$N \rightarrow N$

and zero on “down” triangles (or vice versa, depending on the chirality). The half-filling of the vortices becomes manifest upon reexpressing the dual Hamiltonian in terms of an *unconstrained* electric field as follows:

$$\tilde{\mathcal{H}}_{\text{dual}} = \mathcal{H}_{\text{dual}} + \sum_{\mathbf{x}\mathbf{x}'} (N_{\mathbf{x}} - 1/2)V_{\mathbf{x}\mathbf{x}'}(N_{\mathbf{x}'} - 1/2), \quad (11)$$

where  $V_{\mathbf{x}\mathbf{x}'}$  encodes the logarithmic vortex repulsion. Equation (11) clearly exhibits a vortex particle-hole symmetry.

The transformation properties of the dual fields under the discrete microscopic symmetries can be straightforwardly deduced as discussed in Ref. 25. These are summarized in Table I. The continuous U(1) spin symmetry, which reflects conservation of  $S^z$ , is not directly manifest in this formulation and is instead replaced by a conservation of dual gauge flux,  $(\Delta \times a)$ . Additionally, the dual Hamiltonian has a U(1) gauge redundancy, being invariant under  $(a_{\mathbf{x}\mathbf{x}'} + a_{\mathbf{x}\mathbf{x}'}) \rightarrow (a_{\mathbf{x}\mathbf{x}'} + a_{\mathbf{x}\mathbf{x}'}) + \Lambda_{\mathbf{x}} - \Lambda_{\mathbf{x}'}$  and  $\theta_{\mathbf{x}} \rightarrow \theta_{\mathbf{x}} + \Lambda_{\mathbf{x}}$  for arbitrary  $\Lambda_{\mathbf{x}} \in \mathbb{R}$ .

### III. FERMIONIZED-VORTEX FORMULATION

Due to the finite vortex density together with the strong vortex interactions, the dual theory as it stands appears as intractable as the original spin model. There is, however, an important distinction between the dual vortex formulation and the original hard-core boson representation of the spin model that we can exploit. In the dual theory the vortices move in the presence of a dynamical gauge field which encodes the motion of the hard-core bosons. Thus, the dual vortex theory is in some sense a two-fluid model that describes simultaneously both the dynamics of the hard-core bosons and the vortices. As such, it is possible to imagine a vortex moving together with a cloud of dual gauge flux,  $(\Delta \times a)$ , which can in effect modify the statistics of the vortex-flux composite. Indeed, if the flux has strength  $\pm 2\pi$ , the composite particle will behave like a fermion due to the Aharonov-Bohm phase acquired from the dual flux under an exchange process. What we imagine is that the motion of the vortices and the dual flux can become dynamically correlated in such a fashion to be well represented (on intermediate length scales) by the dynamics of fermionic vortex-flux composites moving in the presence of the remaining dynamical gauge flux.

This physical picture can be implemented by splitting the gauge flux into two pieces,  $a \rightarrow a + A$ , and attaching  $2\pi$  flux of  $(\Delta \times A)$  to the vortices with the help of a Chern-Simons term for  $A$ . An unfortunate but apparently unavoidable feature of this Chern-Simons approach is that we must choose the sign of the attached flux, say,  $+2\pi$  rather than  $-2\pi$ . One could contemplate an alternate formulation wherein the sign of the attached Chern-Simons flux is itself a dynamically fluctuating field, but we do not attempt to do so in this paper.

Before proceeding to the details, we pause to comment on the usefulness and limitations of this approach. Working with fermionized vortices is expected to be legitimate for describing physics in regimes where the vortex exchange statistics is unimportant. Consider, for instance, “insulating” phases of the vortices, examples of which include vortex crystals and “valence bond solids.” Such phases were explored in integer-spin systems in Ref. 25, and shown to correspond to magnetically ordered spin states. At the lowest energy scales, vortex density fluctuations are entirely frozen out, rendering their exchange statistics unimportant; whether the vortices are treated as bosonic or fermionic is presumably inconsequential.

On the other hand, once approximations are made to derive a low-energy effective theory as we will do below, the vortex fermionization approach is expected to be least reliable when describing “vortex condensates.” (Such vortex condensates correspond to paramagnetic states of the original spin system.) It is intuitively clear that trying to mimic the physics of Bose condensation will be challenging with fermionic fields, although this was the approach taken to describe any on superconductivity by a number of authors some years back.

Here, we will be most interested in employing the fermionized vortex approach to access the “critical” algebraic vortex liquid. As we shall see, although the vortices are mobile in this phase, due to their long-range interactions vortex density fluctuations will be so strongly suppressed that the Chern-Simons flux attachment will be ineffective at modifying the behavior on long length scales. We will argue that the asymptotic low-energy physics of the algebraic vortex liquid is described by fermionic vortices minimally coupled to a gauge field mediating a long-range interaction (with Maxwell but no Chern-Simons term). This theory is usually referred to as QED3.

#### A. Fermionization

Formally, fermionization can be implemented by treating the vortices as hard-core bosons, replacing  $e^{i\theta_{\mathbf{x}}} \rightarrow b_{\mathbf{x}}^{\dagger}$  and  $N_{\mathbf{x}} \rightarrow b_{\mathbf{x}}^{\dagger} b_{\mathbf{x}} = 0, 1$ , followed by a 2D Jordan-Wigner transformation,<sup>10</sup>

$$b_{\mathbf{x}}^{\dagger} = d_{\mathbf{x}}^{\dagger} \exp\left(i \sum_{\mathbf{x}' \neq \mathbf{x}} \arg(\mathbf{x}, \mathbf{x}') N_{\mathbf{x}'}\right), \quad (12)$$

$$N_{\mathbf{x}} = b_{\mathbf{x}}^{\dagger} b_{\mathbf{x}} = d_{\mathbf{x}}^{\dagger} d_{\mathbf{x}}. \quad (13)$$

Here  $\arg(\mathbf{x}, \mathbf{x}')$  denotes an angle formed by the vector  $\mathbf{x} - \mathbf{x}'$  with respect to an arbitrary fixed axis.

The dual fermionized-vortex Hamiltonian takes the form

TABLE II. Transformation properties of the fields in the dual fermionized-vortex representation. Symmetry properties of  $a^0$ ,  $a$ ,  $e$  are the same as in Table I. In the  $\mathcal{C}$  column,  $j=1,2$  labels one of the two triangular sublattices of the honeycomb, and  $\langle A \rangle$  refers to the mean-field value of  $A_{\mathbf{x}\mathbf{x}'}$ , with  $\langle N_{\mathbf{x}} \rangle = 1/2$ . The additional column  $\mathcal{T}_{\text{ferm}}$  corresponds to the naive time reversal for the lattice fermions and is *not* a symmetry of the vortex Hamiltonian.

	$T_{\delta\mathbf{r}}, R_{\pi}, R_{\pi/3}$ (isotropic limit)	$\tilde{\mathcal{R}}_{\mathbf{x}}$	$\mathcal{C}$	$\mathcal{T}$	$\mathcal{T}_{\text{ferm}}$
$a^0 \rightarrow$	$a^0$	$-a^0$	$-a^0$	$-a^0$	$-a^0$
$a \rightarrow$	$a$	$-a$	$-a$	$-a$	$-a$
$e \rightarrow$	$e$	$e$	$-e$	$e$	$e$
$d_{\mathbf{x}} \rightarrow$	$d$	$d$	$(-1)^j d^\dagger$	$d_{\mathbf{x}} e^{-2i\sum_{\mathbf{x}' \neq \mathbf{x}} \arg(\mathbf{x}, \mathbf{x}') N_{\mathbf{x}'}}$	$d$
$A \rightarrow$	$A$	$-A$	$2\langle A \rangle - A$	$A$	

$$\mathcal{H}_{\text{dual}} = - \sum_{\langle \mathbf{x}_1 \mathbf{x}_2 \rangle} t_{\mathbf{x}_1 \mathbf{x}_2} (d_{\mathbf{x}_1}^\dagger d_{\mathbf{x}_2} e^{-i(a_{\mathbf{x}_1 \mathbf{x}_2} + a_{\mathbf{x}_1 \mathbf{x}_2}^0 + A_{\mathbf{x}_1 \mathbf{x}_2})} + \text{H.c.}) + \mathcal{H}_a, \quad (14)$$

where we have introduced a Chern-Simons field

$$A_{\mathbf{x}_1 \mathbf{x}_2} = \sum_{\mathbf{x}' \neq \mathbf{x}_1, \mathbf{x}_2} [\arg(\mathbf{x}_2, \mathbf{x}') - \arg(\mathbf{x}_1, \mathbf{x}')] N_{\mathbf{x}'}, \quad (15)$$

which in Eq. (14) resides on honeycomb links. Although we have included only nearest-neighbor hopping in the dual vortex Hamiltonian, one could also generically allow for small further-neighbor hopping terms allowed by symmetry. Upon fermionization, such terms similarly involve fermions coupled to a Chern-Simons field defined as in Eq. (15), but with  $\mathbf{x}_1$  and  $\mathbf{x}_2$  further-neighbor sites.

The transformation properties of the fermions and the Chern-Simons field can be deduced by examining Eqs. (12) and (15). Table II summarizes the symmetry properties of all fields in this representation. According to Eq. (12), particle-hole symmetry sends  $d_{\mathbf{x}} \rightarrow d_{\mathbf{x}}^\dagger e^{i\gamma_{\mathbf{x}}}$ , where for nearest-neighbor honeycomb sites  $\mathbf{x}_{1,2}$  the acquired phases satisfy  $\gamma_{\mathbf{x}_1} - \gamma_{\mathbf{x}_2} = \pi - 2\langle A_{\mathbf{x}_1 \mathbf{x}_2} \rangle$ . Here  $\langle A_{\mathbf{x}_1 \mathbf{x}_2} \rangle$  denotes the mean-field value of the Chern-Simons field with  $\langle N_{\mathbf{x}} \rangle = 1/2$  appropriate for half-filled fermions. Since the Chern-Simons flux through a given hexagonal plaquette averages to  $2\pi$ , which is equivalent to zero flux, we take  $\langle A \rangle = 0$  on nearest-neighbor links. Hence, in the table we implement particle-hole symmetry by transforming  $d_{\mathbf{x}} \rightarrow (-1)^j d_{\mathbf{x}}^\dagger$ , where  $j=1,2$  labels one of the two sublattices of the honeycomb. Note also that as discussed in Ref. 25 time reversal acts nonlocally on the fermions, and consequently we do not know how to faithfully realize this symmetry in the continuum theory derived in the next section. In the last column of Table II we provide a modified time reversal,  $\mathcal{T}_{\text{ferm}}$ , which acts locally on the fermion fields and corresponds to naive time reversal for fermions on a lattice.

### B. Vortex mean field and low-energy theory

One advantage of working with fermionized vortices is that there is then a natural route to a low-energy effective theory. Namely, we start by considering a noninteracting “flux-smearred” mean-field state, ignoring fluctuations in the

Chern-Simons and “electromagnetic” gauge fields and replacing the flux by an average background. Since the vortices are at half-filling, the Chern-Simons flux through each hexagon averages to  $2\pi$ , which is equivalent to zero flux on a lattice. Thus, the “flux-smearred” mean-field Hamiltonian describes free fermionic vortices hopping on the honeycomb in a background of  $\pi$  flux (due to  $a_{\mathbf{x}\mathbf{x}'}^0$ ),

$$\mathcal{H}_{\text{MF}} = - \sum_{\langle \mathbf{x}\mathbf{x}' \rangle} t_{\mathbf{x}\mathbf{x}'} (d_{\mathbf{x}}^\dagger d_{\mathbf{x}'} e^{-ia_{\mathbf{x}\mathbf{x}'}^0} + \text{H.c.}). \quad (16)$$

Working out the fermionized-vortex band structure for  $\mathcal{H}_{\text{MF}}$  exposes the important low-energy degrees of freedom in the mean-field theory. Doing so will enable us to derive a continuum mean-field Hamiltonian, which will serve as the foundation on which we construct the full interacting low-energy theory by restoring fluctuations about the flux-smearred mean-field state. To this end, we diagonalize  $\mathcal{H}_{\text{MF}}$  in momentum space assuming the four-site unit cell shown in Fig. 2, choosing a gauge with  $a_{\mathbf{x}\mathbf{x}'}^0 = \pi/4$  directed along the arrows in the figure. Throughout we take as our origin a triangular lattice site denoted by the filled circle in Fig. 2. The band structure consists of four bands, two with positive energy and two with negative energy. Explicitly, the band

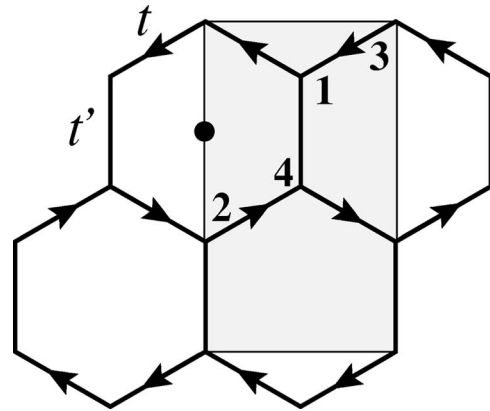


FIG. 2. Four-site unit cell chosen for the honeycomb. With our gauge choice, the static gauge field  $a_{\mathbf{x}\mathbf{x}'}^0$  is zero on the vertical links, while  $a_{\mathbf{x}\mathbf{x}'}^0 = \pi/4$  on the zigzag links directed along the arrows. The filled circle indicates our origin, which coincides with a triangular lattice site.

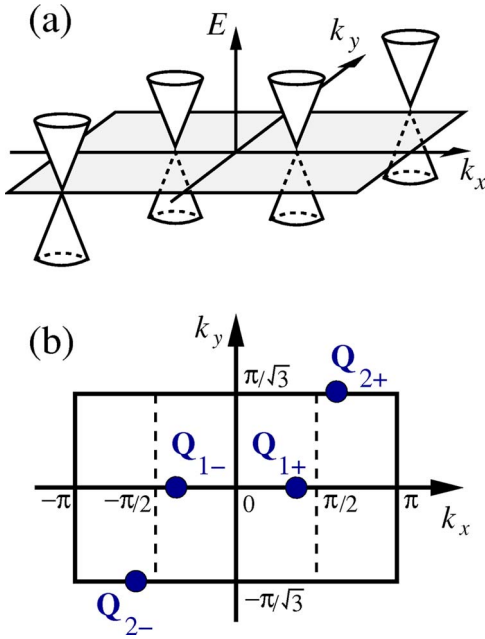


FIG. 3. (Color online) (a) Schematic energy dispersion with  $t'/t < \sqrt{2}$  near the four Dirac points which compose the Fermi “surface” for the half-filled fermions in the flux-smeared mean-field state. (b) Locations of the Dirac points in the rectangular Brillouin zone corresponding to our unit cell choice in Fig. 2. The pairs of nodes  $\mathbf{Q}_{1+}$ ,  $\mathbf{Q}_{1-}$  and  $\mathbf{Q}_{2+}$ ,  $\mathbf{Q}_{2-}$  coalesce when  $t'/t = \sqrt{2}$  and become gapped for  $t'/t > \sqrt{2}$ .

energies at wave vector  $(k_x, k_y)$  in the Brillouin zone of Fig. 3 are given by

$$E^2 = t'^2 + 2t^2 \pm 2t\sqrt{t^2 \sin^2 k_x + t'^2[1 + \cos k_x \cos(\sqrt{3}k_y)]}.$$

The spectrum has Dirac nodes at zero energy for  $t'/t < \sqrt{2}$  and is gapped for  $t'/t > \sqrt{2}$ ; we discuss these two cases separately below. Our main focus will be on the former gapless regime, where the algebraic vortex liquid arises. In the latter case with gapped vortices, which corresponds to the “square-lattice” Néel phase shown in Fig. 4, we will briefly discuss how within our flux-smeared mean-field treatment we can account for the anomalous “roton” minima in the excitation spectra observed by series expansion studies.<sup>27,32</sup>

### 1. $t'/t > \sqrt{2}$ : Gapped vortices. “Rotons” in the frustrated square lattice

For  $t'/t > \sqrt{2}$ , the half-filled fermionic vortices form a band insulator with the minimum band gap occurring at wave vectors  $\mathbf{Q}_1 = (0, 0)$  and  $\mathbf{Q}_2 = (\pi, \pi/\sqrt{3})$  in the Brillouin zone of Fig. 3. It is useful in this range of anisotropy to view the triangular system as a square lattice antiferromagnet with nearest-neighbor exchange  $J'$  and frustrating antiferromagnetic exchange  $J$  along one diagonal direction as shown in Fig. 4. The vortex insulator realized here corresponds to the square-lattice Néel state, which for sufficiently small  $J$  is the anticipated ground state. Since we are considering an easy-plane model, the spins order in the  $(S^x, S^y)$  plane. The gapless Goldstone spin-wave at zero momentum is realized in the dual theory as a propagating “photon” mode in the electro-

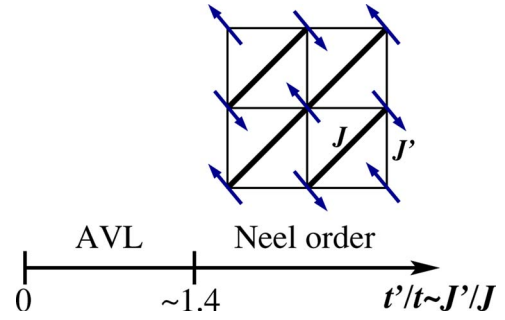


FIG. 4. (Color online) Phase diagram for the dual fermionized-vortex Hamiltonian in the flux-smeared mean-field state. In the range of anisotropy  $t'/t > \sqrt{2}$ , it is useful to view the system as a square lattice antiferromagnet with nearest-neighbor exchange  $J'$  and frustrating coupling  $J$  along one of the diagonal links as shown above.

magnetic gauge fields. (The Goldstone mode at the ordering wave vector present in a Heisenberg system acquires a gap in the easy-plane limit.) The Néel phase survives down to  $t'/t = \sqrt{2}$ , at which point the spectrum becomes gapless at  $\mathbf{Q}_{1,2}$  signaling the destruction of the Néel order. Series expansion studies<sup>32</sup> for the spatially anisotropic Heisenberg system find that the Néel phase survives in a similar range of anisotropy,  $J'/J \gtrsim 1.4$ .

Interestingly, excitation spectra for the Néel state calculated in series expansion studies of the Heisenberg system show significant deviations from spin-wave theory.<sup>27,32</sup> In terms of the standard square-lattice Brillouin zone notation, linear spin-wave theory predicts identical excitation energies at momenta  $(\pi/2, \pi/2)$  and  $(\pi, 0)$  irrespective of the frustrating coupling  $J$ . Series expansions, on the other hand, obtain large energy differences between these momenta due to a “roton” minimum in the spectrum at  $(\pi, 0)$  which deepens as  $J$  increases (see Fig. 3 in Ref. 27). When  $J'/J = 1.7$ , the excitation energy at  $(\pi, 0)$  is roughly 27% lower than that at  $(\pi/2, \pi/2)$ .<sup>27,32</sup>

The anomalous minimum can be accounted for within our flux-smeared mean-field treatment as a low-energy vortex-antivortex excitation, thus substantiating the roton interpretation. Before proceeding, we want to note that Refs. 27 and 32 consider  $S^z = 1$  excitations since the projection of the total spin onto the Néel vector direction (assumed to be along  $S^z$ ) is conserved in the ordered phase of the Heisenberg system. There is no such spin quantum number in the easy-plane case, and we can characterize the excitations only by their momenta. If necessary, in the Heisenberg case there are always low-energy magnons near zero momentum and  $(\pi, \pi)$  which can be added to the vortex-antivortex excitations discussed below to get the required spin quantum number.

To work more formally, consider the dynamical correlation of the  $S^z$  operator at momentum  $\mathbf{q}$  in the flux-smeared mean field theory.  $S^z_{\mathbf{q}}$  obtains contributions from vortex currents whose circulation induces flux in the dual gauge field. The precise form of these vortex currents will be unimportant here, but can be obtained by constructing perturbations to the hopping Hamiltonian which give rise to static gauge flux modulated at wave vector  $\mathbf{q}$ . Generically, these contributions can be expressed as

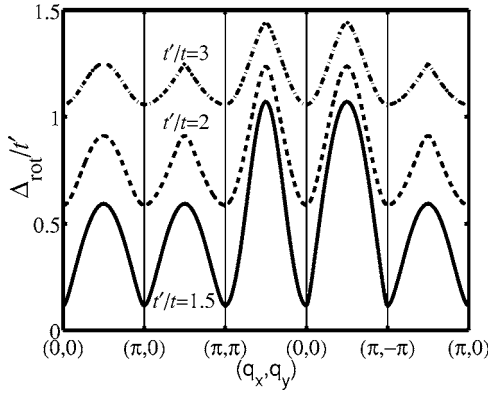


FIG. 5. “Roton” excitation energy  $\Delta_{\text{rot}}(\mathbf{q})$  in the Néel phase along various cuts in momentum space. To facilitate comparison with Fig. 3 from Ref. 27, we use the same square lattice wave vector notation. As frustration increases, the roton excitation energy at  $(\pi, 0)$  decreases, which is consistent with series expansion studies of the Heisenberg system (Refs. 27 and 32), and eventually become *gapless* as the Néel order is destroyed.

$$S_{\mathbf{q}}^z \sim \sum_{a,b=1}^4 \sum_{\mathbf{k}} \gamma_{a,b}(\mathbf{k}, \mathbf{q}) d_a^\dagger(\mathbf{k}) d_b(\mathbf{k} - \mathbf{q}). \quad (17)$$

Here  $a, b$  are band indices,  $\mathbf{k}$  is summed over the Brillouin zone in Fig. 3(b),  $d_a^\dagger(\mathbf{k})$  adds a fermion with momentum  $\mathbf{k}$  in band  $a$ , and  $\gamma_{a,b}$  are generally nonvanishing complex factors. Consequently, the spin structure factor has contributions not only from spin waves, but also from vortex-antivortex “roton” excitations. In the ground state the two lower bands are filled, while the upper bands are empty. The excitation energy  $\Delta_{\text{rot}}(\mathbf{q})$  for a roton with momentum  $\mathbf{q}$  is thus simply given by the minimum energy required to promote a fermion with arbitrary momentum  $\mathbf{k}$  from an occupied band to a state with momentum  $\mathbf{k} - \mathbf{q}$  in an unoccupied band,

$$\Delta_{\text{rot}}(\mathbf{q}) = \min_{\mathbf{k}} [E_{\text{empty}}(\mathbf{k} - \mathbf{q}) - E_{\text{filled}}(\mathbf{k})]. \quad (18)$$

This is straightforward to compute from the vortex band structure. The result for  $\Delta_{\text{rot}}(\mathbf{q})$  along several cuts in momentum space is shown in Fig. 5 for three values of  $t'/t$ . Note that unlike Ref. 27 which shows the lower edge for all excitations including spin waves, our figure shows only the vortex-antivortex excitations. We also point out that the vortex-antivortex excitation energies satisfy  $\Delta_{\text{rot}}(\mathbf{q}) = \Delta_{\text{rot}}[\mathbf{q} + (\pi, 0)] = \Delta_{\text{rot}}[\mathbf{q} + (0, \pi)]$ , though this does not hold for general excitations.

The most notable feature to observe in Fig. 5 is that the roton excitation energy at  $(\pi, 0)$  decreases as the frustration increases, consistent with series expansions, and becomes *gapless* as the Néel order gets destroyed. The roton excitations at  $(0, 0)$  and  $(\pi, \pi)$  follow the same trend, though these low-energy rotons would be difficult to observe in a Heisenberg system due to the gapless spin waves at these momenta. However, since spin waves at  $(\pi, \pi)$  are gapped in the easy-plane limit, significant deviations from spin-wave theory due to the roton at this wave vector are expected. Series expansions for an easy-plane system to search for this anomaly

would be interesting, and could serve as a test for our explanation of the Heisenberg spectra.

## 2. $t'/t < \sqrt{2}$ : Critical vortices

For  $\tilde{t} \equiv t'/t < \sqrt{2}$  one finds that the Fermi “surface” for the half-filled fermionic vortices consists of four gapless, linearly dispersing Dirac points shown schematically in Fig. 3(a). With our gauge choice these Dirac points occur at generally incommensurate wave vectors  $\mathbf{Q}_{1\pm}$  and  $\mathbf{Q}_{2\pm}$  which can be written

$$\mathbf{Q}_{1\pm} = \pm (\pi/2 - \tilde{Q}, 0), \quad (19)$$

$$\mathbf{Q}_{2\pm} = \pm (\pi/2 + \tilde{Q}, \pi/\sqrt{3}), \quad (20)$$

with

$$\tilde{Q} \equiv \frac{\pi}{2} - \cos^{-1} \left( \frac{\tilde{t}^2}{2} \right). \quad (21)$$

Figure 3(b) shows the positions of these wave vectors in the rectangular Brillouin zone corresponding to our unit cell choice. The Dirac points have the familiar relativistic dispersion  $E \approx \pm \sqrt{v_x^2 q_x^2 + v_y^2 q_y^2}$ , where  $\mathbf{q}$  is measured relative to the nodal wave vectors  $\mathbf{Q}_{Ll}$  ( $L=1, 2; l=+, -$ ). The velocities  $v_{x,y}$  are in general anisotropic due to the anisotropy in the hopping amplitudes  $t_{xx'}$  and are given by

$$v_x = t \left( 1 - \frac{\tilde{t}^2}{2} \right)^{1/2}, \quad (22)$$

$$v_y = v_x \left( \frac{3\tilde{t}^4}{4 - \tilde{t}^4} \right)^{1/2}. \quad (23)$$

Note some limiting cases: in the isotropic case  $\tilde{t}=1$  the velocities are equal; in the one-dimensional (1D) limit  $\tilde{t} \rightarrow 0$  the spectrum becomes dispersionless in the  $y$  direction; and finally, as  $\tilde{t} \rightarrow \sqrt{2}$  and we approach the square lattice Néel state, the Dirac cones merge in pairs and flatten in the  $x$  direction, with  $v_x \rightarrow 0$ .

For the purpose of exploring the low-energy physics of the theory, it suffices to focus only on low-energy excitations in the vicinity of the Dirac nodes. This can be achieved by expanding the fermion operators around the wave vectors  $\mathbf{Q}_{Ll}$  as follows:

$$d_{\mathbf{x},\ell} \approx \sum_{L\alpha} e^{i\mathbf{Q}_{Ll} \cdot \mathbf{x}} \Phi_{\ell}^{L\alpha} \psi_{L\alpha}, \quad (24)$$

where  $\mathbf{x}$  denotes sites of the honeycomb as before and  $\ell = 1, \dots, 4$  labels the corresponding site index in the unit cell pictured in Fig. 2. On the right-hand side of Eq. (24),  $\psi_{Ll}$  are two-component spinors assumed to vary slowly on the lattice scale, with spinor components indexed by the label  $\alpha = \uparrow, \downarrow$ . Up to an overall uniform normalization factor, the “eigenvectors”  $\Phi^{L\alpha}$  can be written

TABLE III. Transformation properties of the continuum fermion fields  $\psi$ . Symmetries  $T_1$  and  $T_2$  correspond to translations by  $\delta\mathbf{r}=\hat{\mathbf{x}}$  and  $\delta\mathbf{r}=-1/2\hat{\mathbf{x}}+\sqrt{3}/2\hat{\mathbf{y}}$ , respectively. Moreover,  $\mathcal{T}_{\text{ferm}}$  corresponds to the naive time reversal for fermions on the honeycomb rather than the physical spin time reversal.

	$T_1$	$T_2$	$\tilde{\mathcal{R}}_x$	$R_\pi$	$\mathcal{C}$	$\mathcal{T}_{\text{ferm}}$	$R_{\pi/3}$ (isotropic limit)
$\psi \rightarrow$	$i\tau^z e^{-i\tilde{Q}\mu^z\tau^z}\psi$	$-i\mu^x\tau^y e^{i[(\tilde{Q}/2)-(\pi/4)]\mu^z\tau^z}\psi$	$e^{i(\pi/4)(\mu^z-1)}\psi$	$\tau^x\sigma^z\psi$	$\mu^x\tau^z\sigma^x[\psi^\dagger]^t$	$\mu^y\sigma^y\psi$	$e^{-i(\pi/6)\sigma^z}\mu^x e^{i(\pi/4)\mu^z} e^{i(\pi/4)\mu^x\tau^x}\psi$

$$\begin{aligned}
\Phi^{1+\uparrow} &= \begin{bmatrix} -\tilde{t} \\ s \\ 0 \\ 0 \end{bmatrix}, & \Phi^{1+\downarrow} &= \begin{bmatrix} 0 \\ 0 \\ -\tilde{t} \\ s \end{bmatrix}, \\
\Phi^{1-\uparrow} &= \begin{bmatrix} 0 \\ 0 \\ s \\ -\tilde{t} \end{bmatrix}, & \Phi^{1-\downarrow} &= \begin{bmatrix} -s \\ \tilde{t} \\ 0 \\ 0 \end{bmatrix}, \\
\Phi^{2+\uparrow} &= e^{-i(\pi/12)} \begin{bmatrix} 0 \\ 0 \\ -i\tilde{t} \\ s \end{bmatrix}, & \Phi^{2+\downarrow} &= e^{i(\pi/12)} \begin{bmatrix} -i\tilde{t} \\ -s \\ 0 \\ 0 \end{bmatrix}, \\
\Phi^{2-\uparrow} &= e^{-i(\pi/12)} \begin{bmatrix} s \\ -i\tilde{t} \\ 0 \\ 0 \end{bmatrix}, & \Phi^{2-\downarrow} &= e^{i(\pi/12)} \begin{bmatrix} 0 \\ 0 \\ s \\ i\tilde{t} \end{bmatrix}, \quad (25)
\end{aligned}$$

where  $s \equiv 2 \sin(\tilde{Q}/2)$ .

Using the expansion for the fermion operators in Eq. (24), we obtain the following low-energy continuum description for the mean-field Hamiltonian:

$$\mathcal{H}_{\text{MF}} \sim \int d\mathbf{x} \psi_{LI}^\dagger (-iv_x \partial_x \sigma^x - iv_y \partial_y \sigma^y) \psi_{LI}, \quad (26)$$

where the flavor indices  $LI$  are implicitly summed and  $\sigma^{x,y}$  are Pauli matrices that contract with the spinor indices [i.e.,  $(\sigma^x \psi)_{L\alpha} \equiv \sigma_{\alpha\beta}^x \psi_{L\beta}$ ]. Proceeding to the imaginary-time path integral formulation, the Euclidean-Lagrangian density obtained from Eq. (26) can be written

$$\mathcal{L}_{\text{MF}} \sim \bar{\psi}_{LI} \gamma^\mu \partial_\mu \psi_{LI}, \quad (27)$$

$$\bar{\psi}_{LI} \equiv \psi_{LI}^\dagger \gamma^0, \quad (28)$$

where the space-time index  $\mu=0,1,2$  is defined so that  $\partial_{0,1,2} \equiv \partial_{\tau,x,y}$  and we have rescaled the spatial coordinates to absorb the anisotropic velocities  $v_{x,y}$ . The Dirac matrices  $\gamma^\mu$  are given by  $\gamma^0 = \sigma^z$ ,  $\gamma^1 = \sigma^y$ ,  $\gamma^2 = -\sigma^x$  and satisfy the usual algebra  $\{\gamma^\mu, \gamma^\nu\} = 2\delta^{\mu\nu}$ . We will also frequently use Pauli matrices  $\mu^k$  and  $\tau^k$  which contract with the flavor indices  $L$  and  $l$ , i.e.,

$$(\mu^k \psi)_{LI} \equiv \mu_{LM}^k \psi_{MI},$$

$$(\tau^k \psi)_{LI} \equiv \tau_{lm}^k \psi_{Lm}. \quad (29)$$

Upon resurrecting the vortex interactions and gauge field fluctuations about the mean-field state, we obtain the desired low-energy theory,

$$\begin{aligned}
\mathcal{L} &= \bar{\psi}_{LI} \gamma^\mu (\partial_\mu - ia_\mu - iA_\mu) \psi_{LI} + \frac{1}{2e^2} (\epsilon_{\mu\nu\lambda} \partial_\nu a_\lambda)^2 \\
&+ \frac{i}{4\pi} \epsilon_{\mu\nu\lambda} A_\mu \partial_\nu A_\lambda + \mathcal{L}_{4f}. \quad (30)
\end{aligned}$$

Equation (30) describes four flavors of two-component Dirac fermions  $\psi_{LI}$  (corresponding to the four Dirac points) minimally coupled to a noncompact U(1) gauge field  $a_\mu$  and a Chern-Simons field  $A_\mu$ . The gauge field  $a_\mu$  mediates the logarithmic vortex repulsion, while the Chern-Simons terms above enforce the flux attachment to the fermions, thereby restoring the original bosonic vortex exchange statistics. The form of the Maxwell term above is only schematic and ignores the underlying lattice anisotropy. Finally,  $\mathcal{L}_{4f}$  represents symmetry-allowed four-fermion terms arising from short-range parts of the vortex interactions in the microscopic model. We furnish an explicit form of  $\mathcal{L}_{4f}$  in Sec. V.

Table III displays the transformation properties of the continuum fermion fields under the microscopic symmetries (with  $\mathcal{T}_{\text{ferm}}$  rather than  $\mathcal{T}$  due to subtleties mentioned above). With our gauge choice for  $a_{\mathbf{x}\mathbf{x}'}$  in Fig. 2, the two translations given in Table III are realized as follows. The first,  $T_1$ , corresponds to a simple translation of fields by  $\delta\mathbf{r}=\hat{\mathbf{x}}$ . The second,  $T_2$ , corresponds to translation by  $\delta\mathbf{r}=-1/2\hat{\mathbf{x}}+\sqrt{3}/2\hat{\mathbf{y}}$  and must be accompanied by a gauge transformation. Specifically,  $T_2$  is realized by first implementing the required gauge transformation by sending

$$d_{\mathbf{x},1/4} \rightarrow ie^{i\pi(n_x+n_y)} d_{\mathbf{x},1/4}, \quad (31)$$

$$d_{\mathbf{x},2/3} \rightarrow e^{i\pi(n_x+n_y)} d_{\mathbf{x},2/3}, \quad (32)$$

where  $n_{x,y}$  are integers labeling the unit cell to which site  $\mathbf{x}$  belongs, and then translating as follows:

$$d_{\mathbf{x},1/2} \rightarrow d_{\mathbf{x}+\delta\mathbf{r},2/1}, \quad (33)$$

$$d_{\mathbf{x},3/4} \rightarrow d_{\mathbf{x}+\delta\mathbf{r},4/3}. \quad (34)$$

Particle-hole symmetry and fermionic time reversal similarly require gauge transformations, as do rotations in the isotropic limit  $J=J'$ .

Translations, reflections, and particle-hole symmetry prohibit all possible fermion bilinears from appearing in Eq. (30) except  $i\bar{\psi}\mu^z\tau^z\psi = \psi^\dagger\mu^z\tau^z\sigma^x\psi$  and  $\bar{\psi}\psi = \psi^\dagger\sigma^z\psi$ . The first of these bilinears is a perturbation to the Hamiltonian which

modifies the ratio of vortex hopping amplitudes  $t'/t$ . This has the trivial effect of shifting the  $x$  components of the nodal wave vectors  $\mathbf{Q}_{LI}$ , which are not protected in an anisotropic system. In the isotropic limit,  $i\bar{\psi}\mu^z\tau^z\psi$  is eliminated by rotation symmetry. Deducing the fate of  $\bar{\psi}\psi$ , which respects all symmetries except  $\mathcal{T}_{\text{ferm}}$ , requires more care and will be discussed in Sec. IV A. We will argue that adding this term to the action drives the system into the Kalmeyer-Laughlin chiral spin-liquid, which breaks physical time-reversal symmetry. Thus  $\bar{\psi}\psi$  should be excluded if we are to describe a time-reversal invariant state.

At this point it is worth emphasizing that upon considering the simplest flux-smearred state, we have already arrived at a mean-field description of the “critical” algebraic vortex liquid (AVL) which is the main focus of this paper. The “critical” nature of this state follows from the gaplessness of the fermionic vortices, which in turn allows for gapless spin excitations as we will discuss below. Many properties of the AVL, such as the momentum-space locations of the low-energy spin excitations, can in fact be deduced from the mean-field theory. By studying the effective Lagrangian Eq. (30), we will attempt to go beyond such a mean-field analysis. In particular, in the following section we will address the stability of the AVL when fluctuations about the flux-smearred state are incorporated and make quantitative predictions for various spin correlations in the AVL. Moreover, with this effective theory in hand we can also explore the phase diagram in the vicinity of the AVL. The algebraic vortex liquid has a number of interesting proximate phases, some of which we explore in Sec. V.

To summarize, the mean-field phase diagram along the spatial anisotropy axis  $t'/t$  is shown in Fig. 4. We will focus on  $t'/t < \sqrt{2}$  for the remainder of the paper.

## IV. ALGEBRAIC VORTEX LIQUID

### A. Effective theory of the AVL—QED3

We begin our detailed characterization of the algebraic vortex liquid by examining the continuum theory describing fluctuations about the critical flux-smearred mean-field state. The full interacting theory is described by the effective Lagrangian Eq. (30). To ascertain response properties of the spin system, we add an external probing field  $A^{\text{ext}}$  which couples to the three-current of the hard-core bosons. In the dual vortex formulation prior to fermionization, this three-current is given by  $\delta j = (\nabla \times a)/2\pi$ . Upon fermionization, we introduced an additional Chern-Simons field, and attached flux  $(\nabla \times A) = 2\pi$  to the vortices. As discussed at the beginning of Sec. III, it is convenient to view the Chern-Simons field as being “part” of the original gauge field, that is  $a \rightarrow \tilde{a} = a + A$ . The idea is that it is the physical hard-core boson current which is becoming correlated with the motion of the vortices, forming a vortex-flux composite which behaves as a fermion. Based on this picture, it is reasonable to assume that the Chern-Simons gauge flux carries the  $U(1)$  charge of the hard-core bosons, and to couple in the external field via

$$\mathcal{L}_{\text{ext}} = -\frac{i}{2\pi} A^{\text{ext}} [(\nabla \times a) + (1 - \kappa)(\nabla \times A)], \quad (35)$$

with  $\kappa=0$ . Traditional application of Chern-Simons theory would take instead  $\kappa=1$ , which corresponds to the assump-

tion that the Chern-Simons flux is “fictitious” rather than physical and hence carries no quantum numbers. As we shall see below, the choice  $\kappa=0$  is preferable, being essentially equivalent to replacing physical time reversal invariance by  $\mathcal{T}_{\text{ferm}}$ . But for now we keep  $\kappa$  as an arbitrary parameter.

Since the Dirac fermions in the low-energy continuum theory given in Eq. (30) couple only to  $\tilde{a}_\mu = a_\mu + A_\mu$ , it is instructive to rewrite the Lagrangian in terms of this sum field. The full Lagrangian can then be cast in the following appealing form:

$$\mathcal{L} = \mathcal{L}_{\text{QED3}} + \mathcal{L}_{\text{CS}} + \mathcal{L}_{\text{int}} + \mathcal{L}_{\text{ext}}, \quad (36)$$

with

$$\mathcal{L}_{\text{QED3}} = \bar{\psi}_{LI} \gamma^\mu (\partial_\mu - i\tilde{a}_\mu) \psi_{LI} + \frac{1}{2e^2} (\nabla \times \tilde{a})^2 + \mathcal{L}_{4f}, \quad (37)$$

and

$$\mathcal{L}_{\text{CS}} = \frac{i}{4\pi} A(\nabla \times A). \quad (38)$$

Here,  $\mathcal{L}_{\text{QED3}}$  describes noncompact quantum electrodynamics in 2+1 dimensions (QED3) with  $N=4$  flavors, which is coupled to the Chern-Simons Lagrangian by an interaction,

$$\mathcal{L}_{\text{int}} = -\frac{1}{e^2} (\nabla \times \tilde{a})(\nabla \times A). \quad (39)$$

The external probing field takes the form

$$\mathcal{L}_{\text{ext}} = -\frac{i}{2\pi} A^{\text{ext}} (\nabla \times \tilde{a}) + \kappa \frac{i}{2\pi} A^{\text{ext}} (\nabla \times A). \quad (40)$$

Notice that with the choice  $\kappa=0$ , the external source field only couples to  $\tilde{a}$ .

Before discussing the effects of the interaction term, we briefly review the behavior of QED3, which has been widely studied in a variety of contexts.<sup>25,33–40</sup> The fixed point with  $e^2=0$  in which gauge fluctuations are entirely suppressed and the fermions are essentially free is unstable, so that QED3 is inherently a strongly interacting field theory. Consequently, to make progress analytically one must modify the theory in a manner which provides a controlled limit. An often used approach is the large- $N$  limit, where one generalizes to a large number  $N$  of fermion flavors. Starting from the infinite- $N$  limit, one can then perform a controlled analysis by perturbing in powers of  $1/N$ . This approach can be cast in the form of a renormalization group treatment, and an important feature is that the gauge field  $\tilde{a}$  scales like an inverse length and due to gauge invariance does not pick up an anomalous dimension. The scaling dimensions of the symmetry-allowed four-fermion interactions in Eq. (37) do generally acquire an anomalous dimension, which can be computed perturbatively in inverse powers of  $N$ . For large enough  $N$  all four-fermion terms are irrelevant, and QED3 thus realizes a nontrivial stable critical phase. For  $N < N_c$ , with some unknown  $N_c$ , it is believed that four-fermion terms become relevant, leading to spontaneous fermion mass generation and the destruction of criticality (except with fine-tuning). While  $N_c$  can in principle be deduced in QED3 simulations, recent studies are inconclusive as to whether  $N_c$  lies above or below the  $N=4$

case of interest in the present work.<sup>39,40</sup> We will assume henceforth that  $N_c < 4$ . Further numerical simulations and higher-order calculations in  $1/N$  would be useful for justifying (or negating) this assumption.

We are now in position to consider the effects of the coupling  $\mathcal{L}_{\text{int}}$  between QED3 and the Chern-Simons Lagrangian. Since  $\mathcal{L}_{\text{CS}}$  is Gaussian, it can be viewed as the fixed point of a renormalization group transformation in which  $A$  is rescaled like an inverse length. For large  $e$ , the effects of the interaction can then be studied perturbatively. Since  $\mathcal{L}_{\text{int}}$  is quadratic in the gauge fields and involves two derivatives it has scaling dimension 4, and is formally irrelevant. The fixed points described by QED3 and Chern-Simons theory evidently decouple at low energies. The physics here is that due to the logarithmic vortex repulsion which strongly suppresses vortex density fluctuations, exchange statistics play only a minor role at criticality. In the next section we will employ QED3 to access the properties of the critical algebraic vortex liquid phase.

But caution is necessary. For  $\mathcal{L}_{\text{QED3}}$  fermionic time reversal symmetry precludes the generation of a fermionic mass term  $\bar{\psi}\psi$ , which respects all symmetries of the Lagrangian except  $\mathcal{T}_{\text{ferm}}$ . The Chern-Simons Lagrangian  $\mathcal{L}_{\text{CS}}$ , however, is not invariant under  $\mathcal{T}_{\text{ferm}}$ . As a result, once the two theories are coupled, despite the irrelevance of this coupling a small fermion mass term will presumably be generated, being no longer symmetry protected. Tracing back its origin, we see that the sign of the vortex mass will be determined by the sign of the flux that was attached upon vortex fermionization. As we will discuss in Sec. V A, this mass term drives the system into the Kalmeyer-Laughlin chiral spin-liquid, which breaks *physical* spin time-reversal symmetry. Thus, in order to correctly implement a renormalization group analysis that faithfully respects the physical time-reversal symmetry of the original spin model, we must maintain masslessness of the fermions. We will proceed under the assumption that the physically correct procedure is to tune a small bare mass term to cancel the effects of the irrelevant coupling as it scales to zero—that is, to tune the fully renormalized mass term to zero. The resulting massless and critical QED3 gives us a description of the time-reversal invariant algebraic vortex liquid.

Subtleties associated with time-reversal invariance are also apparent in the Hall conductivity of the original hard-core bosons, which we now briefly discuss. Once the Chern-Simons Lagrangian  $\mathcal{L}_{\text{CS}}$  has decoupled, one can readily perform the Gaussian integration over  $A$ , which gives

$$\mathcal{L}_{\text{ext}} = -\frac{i}{2\pi} A^{\text{ext}}(\nabla \times \tilde{a}) - \kappa^2 \frac{i}{4\pi} A^{\text{ext}}(\nabla \times A^{\text{ext}}). \quad (41)$$

This form shows that the conductivity tensor of the original hard-core bosons,  $\sigma_{\alpha\beta}$ , is given by

$$\sigma_{\alpha\beta} = \frac{\rho_{\alpha\beta}^{\text{fv}}}{(2\pi)^2} + \frac{\kappa^2}{2\pi} \epsilon_{\alpha\beta}, \quad (42)$$

where  $\rho^{\text{fv}}$  is the resistivity tensor for the fermionic vortices described by QED3 and  $\epsilon$  is the antisymmetric tensor. Since the Hall resistivity for the fermions vanishes in QED3 due to

$\mathcal{T}_{\text{ferm}}$  symmetry, the Hall conductivity for the bosons in the critical AVL phase is given by  $\sigma_{xy} = \kappa^2/2\pi$ . Recall that the parameter  $\kappa$  gives a measure of how much bosonic charge is ascribed to the statistical flux attached to the vortices.

Generally, the Hall conductivity is *not* a low-energy property of a physical system, and as such can be nonuniversal even at a critical point or in a critical phase. However, since the original spin model is time-reversal invariant, the Hall conductivity must vanish, at least in the absence of any spontaneous symmetry breaking. Notice that the required vanishing of the Hall conductivity follows provided we take the parameter  $\kappa=0$ . As discussed above and in Sec. III, the choice  $\kappa=0$  corresponds to assuming that the Chern-Simons flux attached to the vortices carries a nonvanishing boson charge. On the other hand, if the statistical flux is presumed to carry no charge, one has  $\kappa=1$  and a nonvanishing Hall conductivity, with a sign set by the sign of the attached statistical flux. The former choice,  $\kappa=0$ , gives us a way to access a time-reversal invariant state with zero Hall conductivity independent of the sign of attached flux. Physically, with the fermions coupling to the sum  $\tilde{a}=a+A$ , the motion of the vortices leads to a “screening” of the attached flux  $\nabla \times A$ , by the fluctuating flux  $\nabla \times a$ . At long wavelengths the total flux surrounding each vortex,  $\nabla \times \tilde{a}$ , which is proportional to the full boson current when  $\kappa=0$ , vanishes. The vortices are charge neutral and the Hall effect vanishes.

It would clearly be desirable to have a method for fermionization involving flux attachment in a more democratic fashion which treats  $+2\pi$  and  $-2\pi$  in an exactly equivalent manner. But in the absence of such an approach, we must content ourselves with using  $\mathcal{L}_{\text{QED3}}$  together with the assumption of  $\kappa=0$  to describe the properties of the time-reversal invariant AVL phase.

## B. Symmetries of the AVL

The critical QED3 theory proposed to describe the AVL respects all symmetries in Table III, and also has a dual global U(1) symmetry under  $\psi \rightarrow e^{i\alpha}\psi$  reflecting conservation of vorticity. Due to the assumed irrelevance of four-fermion terms in the scaling limit, the theory also possesses an emergent global SU(4) flavor symmetry, being invariant under arbitrary SU(4) flavor rotations of the form  $\psi \rightarrow U\psi$ , with  $U^\dagger = U^{-1}$ . The 16 conserved three-currents associated with the U(1) and SU(4) symmetries can be compactly written

$$J_{\alpha\beta}^\nu = \bar{\psi} \gamma^\nu \mu^\alpha \tau^\beta \psi \quad (43)$$

and satisfy  $\partial_\nu J_{\alpha\beta}^\nu = 0$ . Here the indices  $\alpha, \beta$  range from 0 to 3;  $\mu^0$  and  $\tau^0$  are identity matrices; and  $\mu^i$  and  $\tau^i$  are Pauli matrices defined as in Eq. (29). The U(1) conserved current is  $J_{00}^\nu$ , while the remaining 15 currents constitute the SU(4) conserved currents. The 48 fermion bilinears comprising  $J_{\alpha\beta}^\nu$  are prohibited from acquiring an anomalous dimension. We will be primarily interested in the remaining 16 bilinears, whose correlations are enhanced by gauge fluctuations; their transformation properties are supplied in Table IV. Figure 6 displays the set of momenta carried by these enhanced fermion bilinears, which correspond to the leading gapless

TABLE IV. Transformation properties of the 16 bilinears whose correlations are enhanced by gauge fluctuations at the AVL fixed point (we do not show separately  $\mathcal{M}_{SS}^\dagger$  and  $\mathcal{P}_{1,2,3}^\dagger$ ). In the second column,  $\mathbf{Q}$  is the spiral ordering wave vector defined in Eq. (44),  $\mathbf{K}_j$  lie on the midpoints of the Brillouin zone edges, and  $\mathbf{P}_j = \mathbf{Q} + \mathbf{K}_j$ . Figure 6 displays the set of momenta carried by the enhanced fermion bilinears.

	$T_{\delta\mathbf{r}}$	$\tilde{\mathcal{R}}_x$	$R_\pi$	$\mathcal{C}$	$T_{\text{ferm}}$	$R_{\pi/3}$ (isotropic limit)
$\bar{\psi}\psi = \mathcal{M}_{KL} \rightarrow$	$\mathcal{M}_{KL}$	$\mathcal{M}_{KL}$	$\mathcal{M}_{KL}$	$\mathcal{M}_{KL}$	$-\mathcal{M}_{KL}$	$\mathcal{M}_{KL}$
$\bar{\psi}\mu^z\tau^z\psi = \mathcal{M}_{\sqrt{3}\times\sqrt{3}} \rightarrow$	$\mathcal{M}_{\sqrt{3}\times\sqrt{3}}$	$\mathcal{M}_{\sqrt{3}\times\sqrt{3}}$	$-\mathcal{M}_{\sqrt{3}\times\sqrt{3}}$	$-\mathcal{M}_{\sqrt{3}\times\sqrt{3}}$	$\mathcal{M}_{\sqrt{3}\times\sqrt{3}}$	$-\mathcal{M}_{\sqrt{3}\times\sqrt{3}}$
$\bar{\psi}(\tau^x + i\mu^z\tau^y)\psi = \mathcal{M}_{SS} \rightarrow$	$e^{i\mathbf{Q}\cdot\delta\mathbf{r}}\mathcal{M}_{SS}$	$\mathcal{M}_{SS}$	$\mathcal{M}_{SS}^\dagger$	$-\mathcal{M}_{SS}$	$-\mathcal{M}_{SS}^\dagger$	$\mathcal{M}_{SS}^\dagger$
$\bar{\psi}\mu^x\tau^x\psi = \mathcal{K}_1 \rightarrow$	$e^{i\mathbf{K}_1\cdot\delta\mathbf{r}}\mathcal{K}_1$	$\mathcal{K}_2$	$\mathcal{K}_1$	$-\mathcal{K}_1$	$\mathcal{K}_1$	$\mathcal{K}_3$
$\bar{\psi}\mu^y\tau^y\psi = \mathcal{K}_2 \rightarrow$	$e^{i\mathbf{K}_2\cdot\delta\mathbf{r}}\mathcal{K}_2$	$\mathcal{K}_1$	$\mathcal{K}_2$	$-\mathcal{K}_2$	$\mathcal{K}_2$	$\mathcal{K}_1$
$\bar{\psi}\mu^z\psi = \mathcal{K}_3 \rightarrow$	$e^{i\mathbf{K}_3\cdot\delta\mathbf{r}}\mathcal{K}_3$	$\mathcal{K}_3$	$\mathcal{K}_3$	$-\mathcal{K}_3$	$\mathcal{K}_3$	$\mathcal{K}_2$
$\bar{\psi}\mu^y\tau^y\psi = \mathcal{K}'_1 \rightarrow$	$e^{i\mathbf{K}_1\cdot\delta\mathbf{r}}\mathcal{K}'_1$	$-\mathcal{K}'_2$	$-\mathcal{K}'_1$	$\mathcal{K}'_1$	$-\mathcal{K}'_1$	$\mathcal{K}'_3$
$\bar{\psi}\mu^x\tau^x\psi = \mathcal{K}'_2 \rightarrow$	$e^{i\mathbf{K}_2\cdot\delta\mathbf{r}}\mathcal{K}'_2$	$-\mathcal{K}'_1$	$-\mathcal{K}'_2$	$\mathcal{K}'_2$	$-\mathcal{K}'_2$	$\mathcal{K}'_1$
$\bar{\psi}\tau^z\psi = \mathcal{K}'_3 \rightarrow$	$e^{i\mathbf{K}_3\cdot\delta\mathbf{r}}\mathcal{K}'_3$	$\mathcal{K}'_3$	$-\mathcal{K}'_3$	$\mathcal{K}'_3$	$-\mathcal{K}'_3$	$-\mathcal{K}'_2$
$\bar{\psi}(\mu^x + i\mu^y\tau^z)\psi = \mathcal{P}_1 \rightarrow$	$e^{i\mathbf{P}_1\cdot\delta\mathbf{r}}\mathcal{P}_1$	$\mathcal{P}_2$	$\mathcal{P}_1^\dagger$	$\mathcal{P}_1$	$\mathcal{P}_1^\dagger$	$\mathcal{P}_3^\dagger$
$\bar{\psi}(\mu^y - i\mu^x\tau^z)\psi = \mathcal{P}_2 \rightarrow$	$e^{i\mathbf{P}_2\cdot\delta\mathbf{r}}\mathcal{P}_2$	$\mathcal{P}_1$	$\mathcal{P}_2^\dagger$	$\mathcal{P}_2$	$\mathcal{P}_2^\dagger$	$\mathcal{P}_1^\dagger$
$\bar{\psi}(\mu^z\tau^x + i\tau^y)\psi = \mathcal{P}_3 \rightarrow$	$e^{i\mathbf{P}_3\cdot\delta\mathbf{r}}\mathcal{P}_3$	$\mathcal{P}_3$	$\mathcal{P}_3^\dagger$	$\mathcal{P}_3$	$\mathcal{P}_3^\dagger$	$\mathcal{P}_2^\dagger$

vortex-antivortex excitations. The wave vectors in the figure are explicitly given by  $\pm\mathbf{Q}$ , where

$$\mathbf{Q} = (2\tilde{Q} + \pi, 0) \quad (44)$$

and  $\tilde{Q}$  is defined in Eq. (21),  $\mathbf{K}_{1,2} = (\pi, \mp\pi/\sqrt{3})$ ,  $\mathbf{K}_3 = (0, 2\pi/\sqrt{3})$ , and  $\pm\mathbf{P}_j = \pm(\mathbf{Q} + \mathbf{K}_j)$ . We will often refer to  $\pm\mathbf{Q}$  as spiral ordering wave vectors, since in the isotropic limit these correspond to the  $\sqrt{3} \times \sqrt{3}$  order.

### C. Dynamical spin correlations in the AVL

We turn now to the dynamical spin correlations in the AVL. Due to the gaplessness of the fermionic vortices, the AVL admits universal power-law correlations in the spin structure factor. To extract these spin correlations from our dual theory, we need to first identify the operators in QED3

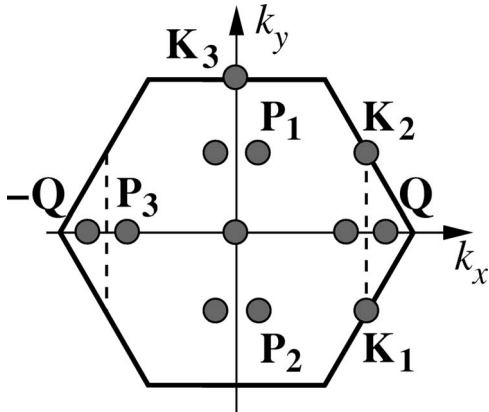


FIG. 6. Momenta carried by the fermion bilinears in Table IV, whose correlations are enhanced by gauge fluctuations at the AVL fixed point.

which correspond to  $S^z$  and  $S^+$ . We discuss the correlations of  $S^z$  and  $S^+$  separately below.

#### 1. $S^z$ correlators

From our microscopic identification in Eq. (7), it is clear that near zero momentum  $S^z$  appears in QED3 as the conserved dual gauge flux,  $(\nabla \times a)/2\pi$ . Since  $a$  is massless in the critical theory,  $S^z$  exhibits power-law correlations at zero momentum with scaling dimension 2. At other wave vectors,  $S^z$  receives contributions from fermion bilinears in QED3 which carry the same quantum numbers. More precisely, due to subtleties with realizing physical time reversal in QED3, we require that contributing fermion bilinears have the same quantum numbers as  $\nabla \times a$ . These bilinears arise microscopically from gapless vortex currents that induce gauge flux modulations at finite wave vector, which are analogous to the “rotons” discussed in Sec. III B 1.

From such an analysis, the continuum expression for  $S^z$  takes the form

$$S^z \sim \frac{\Delta \times a}{2\pi} + (e^{i\mathbf{Q}\cdot\mathbf{r}}\mathcal{M}_{SS} + \text{H.c.}) + \dots, \quad (45)$$

where  $\mathcal{M}_{SS}$  and  $\mathcal{M}_{SS}^\dagger$  are enhanced fermion bilinears from Table IV that carry momenta  $\pm\mathbf{Q}$ . It can be readily verified using the table that the right-hand side has the desired symmetry properties. The ellipsis in Eq. (45) represents terms arising from nonenhanced fermion bilinears [i.e., those which are part of the SU(4) conserved currents] and higher-order contributions. For completeness, we note that these nonenhanced bilinears carry momenta  $\mathbf{K}_{1,2,3}$  and  $\pm\mathbf{P}_{1,2,3}$  in Fig. 6. Thus the  $S^z$  correlations at momenta  $\mathbf{K}_j$  and  $\pm\mathbf{P}_j$  have scaling dimension  $\Delta_{\text{nonenh}} = 2$ .

Due to enhancement from gauge field fluctuations, the fermion bilinear  $\mathcal{M}_{SS}$  in fact provides the dominant power

TABLE V. Transformation properties of the zero-mode operators  $f_{LL,q}$  in the charge  $q = \pm 1$  monopole sectors. The quoted transformations were obtained by employing the Coulomb gauge for the added  $\pm 2\pi$  gauge flux. Also shown are the transformation properties of the six translation eigenoperators  $F_{\alpha,q}^\dagger$  defined in Eq. (52) which add fermions to two of the four zero modes.

	$T_1$	$T_2$	$\tilde{\mathcal{R}}_x$	$R_\pi$	$\mathcal{C}$	$\mathcal{T}_{\text{ferm}}$	$R_{\pi/3}$ (isotropic limit)
$f_q \rightarrow$	$i\tau^z e^{-i\tilde{Q}\mu^z\tau^z} f_q$	$-i\mu^x \tau^y e^{i[(\tilde{Q}/2) - (\pi/4)]\mu^z\tau^z} f_q$	$e^{i(\pi/4)(\mu^z-1)} f_q$	$q\tau^x f_q$	$\mu^x \tau^z [f_{-q}^\dagger]^l$	$-iq\mu^y f_{-q}$	$e^{-iq(\pi/6)} \mu^x e^{i(\pi/4)\mu^z} e^{i(\pi/4)\mu^x\tau^z} f_q$
$F_{0,q}^\dagger \rightarrow$	$-F_{0,q}^\dagger$	$-F_{0,q}^\dagger$	$iF_{0,q}^\dagger$	$F_{0,q}^\dagger$	$F_{0,-q}$	$F_{0,-q}^\dagger$	$-e^{iq\pi/3} F_{0,q}^\dagger$
$F_{1,q}^\dagger \rightarrow$	$F_{1,q}^\dagger$	$F_{1,q}^\dagger$	$iF_{2,q}^\dagger$	$-F_{1,q}^\dagger$	$F_{1,-q}$	$F_{1,-q}^\dagger$	$e^{iq\pi/3} F_{3,q}^\dagger$
$F_{2,q}^\dagger \rightarrow$	$F_{2,q}^\dagger$	$-F_{2,q}^\dagger$	$iF_{1,q}^\dagger$	$-F_{2,q}^\dagger$	$F_{2,-q}$	$F_{2,-q}^\dagger$	$e^{iq\pi/3} F_{1,q}^\dagger$
$F_{3,q}^\dagger \rightarrow$	$-F_{3,q}^\dagger$	$F_{3,q}^\dagger$	$iF_{3,q}^\dagger$	$-F_{3,q}^\dagger$	$F_{3,-q}$	$F_{3,-q}^\dagger$	$e^{iq\pi/3} F_{2,q}^\dagger$
$F_{R,q}^\dagger \rightarrow$	$e^{-2i\tilde{Q}} F_{R,q}^\dagger$	$e^{i(\tilde{Q}-\frac{\pi}{2})} F_{R,q}^\dagger$	$iF_{R,q}^\dagger$	$F_{L,q}^\dagger$	$-F_{L,-q}$	$F_{L,-q}^\dagger$	$-e^{iq\pi/3} F_{L,q}^\dagger$
$F_{L,q}^\dagger \rightarrow$	$e^{2i\tilde{Q}} F_{L,q}^\dagger$	$e^{-i(\tilde{Q}-\frac{\pi}{2})} F_{L,q}^\dagger$	$iF_{L,q}^\dagger$	$F_{R,q}^\dagger$	$-F_{R,-q}$	$F_{R,-q}^\dagger$	$-e^{iq\pi/3} F_{R,q}^\dagger$

law in the  $S^z$  correlations. Near momenta  $\pm \mathbf{Q}$  the  $S^{zz}$  spin structure factor scales as

$$S^{zz}(\mathbf{k} = \pm \mathbf{Q} + \mathbf{q}, \omega) \sim \frac{\Theta(\omega^2 - \mathbf{q}^2)}{(\omega^2 - \mathbf{q}^2)^{1-\eta_{\text{enh}}/2}}. \quad (46)$$

The anomalous dimension  $\eta_{\text{enh}}$  is that of an enhanced fermion bilinear in QED3 and can be estimated from the leading  $1/N$  result,<sup>34</sup>

$$\eta_{\text{enh}} \approx 3 - \frac{128}{3\pi^2 N}. \quad (47)$$

Setting  $N=4$  yields  $\eta_{\text{enh}} \approx 1.92$ , and a scaling dimension  $\Delta_{\text{enh}} = (1 + \eta_{\text{enh}})/2 \approx 1.46$ . At all other wave vectors  $S^{zz}$  exhibits subdominant power laws.

The fact that the leading  $S^z$  correlations occur at momenta  $\pm \mathbf{Q}$  suggests proximity of ‘‘supersolids’’ to the AVL. Such states are characterized by concurrent  $S^z$  and  $S^+$  order, and are nontrivial in an easy-plane system where typically only in-plane spin order occurs. As we will show in Sec. V B 2, supersolid phases indeed emerge naturally out of the AVL.

## 2. $S^+$ correlators

Since the spin raising and lowering operators  $S^\pm$  add spin  $\pm 1$ , the corresponding operators in QED3 are ‘‘monopole insertions’’ which add  $\pm 2\pi$  gauge flux. Our goal here will be to construct a continuum expression for  $S^+$  in terms of these monopoles and from this extract the leading in-plane spin correlations, much as we did for  $S^z$  above. Monopole operators in QED3 were discussed in a very similar setting in Ref. 25, and here we shall only highlight the main points. We will assume that the added  $\pm 2\pi$  flux is spread smoothly over a large area compared to the lattice unit cell, and treat the flux as a static background. This flux alters the fermionic spectrum, and in particular gives rise to four zero-energy modes, one for each fermion flavor in the continuum. The zero-mode wave functions can be obtained by first modifying the mean-field Hamiltonian density in Eq. (26) as follows:

$$\mathcal{H}_{\text{MF},q} \sim -i\psi_{LL}^\dagger [(\partial_x - ia_x^q)\sigma^x + (\partial_y - ia_y^q)\sigma^y] \psi_{LL}. \quad (48)$$

Here  $a_{x,y}^q$  is the vector potential giving rise to  $2\pi q$  flux, with  $q = \pm 1$  the monopole ‘‘charge.’’ Focusing only on the zero modes, we then replace

$$\psi_{LL}(\mathbf{x}) \rightarrow \phi_{LL,q}(\mathbf{x}) f_{LL,q}, \quad (49)$$

where  $\phi_{LL,q}$  are the desired zero-mode wave functions and the operator  $f_{LL,q}$  annihilates the corresponding zero mode. Choosing the Coulomb gauge for  $a_{x,y}^q$  and assuming an azimuthally symmetric flux distribution centered around the origin, it is straightforward to show that the zero-mode wave functions are<sup>41</sup>

$$\phi_{LL,+1} \sim \frac{1}{|\mathbf{x}|} \begin{pmatrix} 1 \\ 0 \end{pmatrix}, \quad (50)$$

$$\phi_{LL,-1} \sim \frac{1}{|\mathbf{x}|} \begin{pmatrix} 0 \\ 1 \end{pmatrix}. \quad (51)$$

The transformation properties of the zero-mode operators  $f_{LL,q}$  can be deduced from Eq. (49) and the transformation properties of  $\psi_{LL}$  in Table III; the results are shown in Table V.

Since the fermions are at half-filling, physical (i.e., gauge-invariant) states must have two of the four zero modes occupied. Thus we need to consider six distinct monopole insertions. It will be useful to define the following translation eigenoperators which add fermions to two of the four zero modes:

$$\begin{aligned} F_{0,q}^\dagger &= f_{1+,q}^\dagger f_{2+,q}^\dagger + f_{1-,q}^\dagger f_{2-,q}^\dagger, \\ F_{1,q}^\dagger &= f_{1+,q}^\dagger f_{1-,q}^\dagger + f_{2+,q}^\dagger f_{2-,q}^\dagger, \\ F_{2,q}^\dagger &= -i[f_{1+,q}^\dagger f_{1-,q}^\dagger - f_{2+,q}^\dagger f_{2-,q}^\dagger], \\ F_{3,q}^\dagger &= f_{1-,q}^\dagger f_{2-,q}^\dagger - f_{1+,q}^\dagger f_{2+,q}^\dagger, \\ F_{R,q}^\dagger &= f_{1-,q}^\dagger f_{2+,q}^\dagger, \\ F_{L,q}^\dagger &= f_{1+,q}^\dagger f_{2-,q}^\dagger. \end{aligned} \quad (52)$$

For convenience, the transformation properties of these operators are also displayed in Table V.

We now introduce the monopole operators by specifying their action on the ground state with no added flux, denoted  $|0\rangle$ . First, we define monopole creation operators  $M_\alpha^\dagger$  which

insert  $+2\pi$  flux and fill the zero modes as follows:

$$M_0^\dagger|0\rangle = e^{i\alpha_0}F_{0,+1}^\dagger|DS, +1\rangle, \quad (53)$$

$$M_j^\dagger|0\rangle = e^{i\alpha_j}F_{j,+1}^\dagger|DS, +1\rangle, \quad (54)$$

$$M_{R/L}^\dagger|0\rangle = e^{i\alpha_{R/L}}F_{R/L,+1}^\dagger|DS, +1\rangle, \quad (55)$$

Here  $j$  runs from 1 to 3 and  $|DS, +1\rangle$  is the filled negative-energy Dirac sea with  $+2\pi$  flux inserted and all zero modes vacant. The Hermitian conjugate operators  $M_\alpha$  are required to add the opposite momentum and flux to the ground state,

$$M_0|0\rangle = e^{i\beta_0}F_{0,-1}^\dagger|DS, -1\rangle, \quad (56)$$

$$M_j|0\rangle = e^{i\beta_j}F_{j,-1}^\dagger|DS, -1\rangle, \quad (57)$$

$$M_{R/L}|0\rangle = e^{i\beta_{R/L}}F_{R/L,-1}^\dagger|DS, -1\rangle, \quad (58)$$

where  $|DS, -\rangle$  is the filled negative-energy Dirac sea with  $-2\pi$  flux inserted. It is important to note that the phases  $\alpha$  and  $\beta$  in the definitions above are arbitrary, and can be specified to our convenience so as to construct operators with the desired transformation properties.

To obtain a continuum expression for  $S^+$  in terms of the monopole operators, we need to determine the quantum numbers they carry. This in turn requires knowing the transformation properties of  $|DS, q\rangle\langle 0|$ . We take up this rather involved issue in the Appendix. By employing general relations among the symmetries (such as  $R_\pi^2=1$ , etc.), we first establish that

$$T_{1,2}: |DS, q\rangle\langle 0| \rightarrow -|DS, q\rangle\langle 0|,$$

$$\tilde{R}_x: |DS, q\rangle\langle 0| \rightarrow i\zeta_x|DS, q\rangle\langle 0|,$$

$$R_\pi: |DS, q\rangle\langle 0| \rightarrow \zeta_\pi|DS, q\rangle\langle 0|,$$

$$C: |DS, q\rangle\langle 0| \rightarrow \prod_{Aa} f_{Aa,-q}^\dagger |DS, -q\rangle\langle 0|,$$

$$\mathcal{T}_{\text{ferm}}: |DS, q\rangle\langle 0| \rightarrow |DS, -q\rangle\langle 0|,$$

$$R_{\pi/3}: |DS, q\rangle\langle 0| \rightarrow \zeta_\pi e^{2iq\pi/3}|DS, q\rangle\langle 0|. \quad (59)$$

Here  $\zeta_x$  and  $\zeta_\pi$  are signs which in principle are fixed, but cannot be determined using only symmetry relations. The specified action under rotation applies only in the isotropic limit.

This information is sufficient to determine the momenta carried by the monopoles:  $M_0$  carries zero momentum,  $M_j$  carries momentum  $\mathbf{K}_j$  on the midpoint of a Brillouin zone edge (cf. Fig. 7), and  $M_{R/L}$  carry momenta at the spiral ordering wave vectors  $\pm\mathbf{Q}$ . For other symmetries, however, a more careful analysis is required. In fact, by examining the symmetry of the monopoles under inversion, one can show that it is *impossible* for all six bare monopole operators to contribute to  $S^+$ . Under inversion, we have  $M_0 \rightarrow \zeta_\pi M_0$  while  $M_j \rightarrow -\zeta_\pi M_j$ . But the Fourier components of  $S^+$  at zero mo-

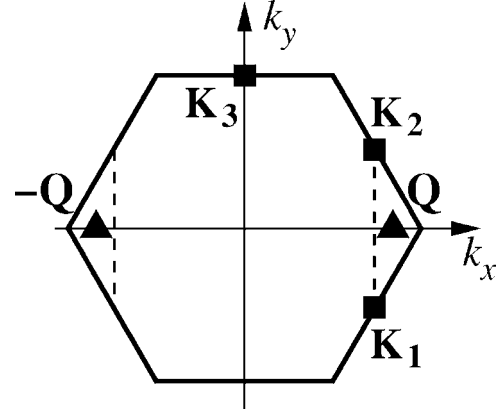


FIG. 7. Momenta at which the dynamical spin structure factor  $S^{+-}$  exhibits dominant power-law correlations with the *same exponent* in the AVL. The leading power law in the  $S^{zz}$  structure factor, by contrast, occurs only at momenta  $\pm\mathbf{Q}$ .

mentum and  $\mathbf{K}_j$  are all *even* under inversion. Depending on the sign  $\zeta_\pi$ , either the bare monopole  $M_0$  or the three monopoles  $M_j$  must therefore be excluded on symmetry grounds from a continuum expression for  $S^+$ . (Since  $M_{R/L}$  are not diagonal under inversion, one can always choose the phases  $\alpha_{R/L}$  and  $\beta_{R/L}$  to construct operators that transform like  $S^+$  at momenta  $\pm\mathbf{Q}$ .)

To determine the remaining ambiguities we appeal to numerical studies of monopole insertions. Specifically, we diagonalize the mean-field hopping Hamiltonian on a finite system with arbitrary flux insertions to obtain the single-particle energies and wave functions. With these wave functions in hand, it is then possible to obtain the inversion and reflection properties of  $|DS, q\rangle\langle 0|$ . These numerics are discussed in more detail in the Appendix. To ensure geometry independence of the results, a variety of boundary conditions and system sizes were considered. In all cases, we find that  $\zeta_\pi = \zeta_x = -1$ . In particular, we conclude that  $M_0$  by itself does not contribute to a continuum expression for  $S^+$ .

We now have enough information to determine unambiguously all quantum numbers carried by the monopoles. It is straightforward to show that the phases appearing in Eqs. (53)–(58) can be chosen so that the monopoles transform as shown in Table VI. [Note that under physical time-reversal  $S^+ \rightarrow -S^-$ , whereas  $\mathcal{T}_{\text{ferm}}$  sends  $M_\alpha^\dagger \rightarrow +M_\alpha$ . This is not too surprising, however, given that the  $U(1)$  spin symmetry is not manifest in the dual theory.] The desired continuum expression for  $S^+$  can then be written as follows:

$$S^+ \sim (e^{-i\mathbf{Q}\cdot\mathbf{r}}M_R^\dagger + e^{i\mathbf{Q}\cdot\mathbf{r}}M_L^\dagger) + \sum_{j=1}^3 e^{i\mathbf{K}_j\cdot\mathbf{r}}M_j^\dagger + \dots, \quad (60)$$

where the ellipsis represents subdominant contributions. The momenta  $\pm\mathbf{Q}$  and  $\mathbf{K}_j$  carried by the monopoles on the right-hand side are sketched in Fig. 7.

Monopole operators are known to have nontrivial power-law correlations in large- $N$  QED3, each with *identical* scaling dimension  $\Delta_m \approx 0.26N$ .<sup>42</sup> This fact leads us to a non-trivial prediction for the in-plane spin structure factor  $S^{+-}$  in the AVL. Namely,  $S^{+-}$  exhibits the same universal power-law

TABLE VI. Transformation properties of the six monopole operators in QED3.

	$T_{\delta\mathbf{r}}$	$\tilde{\mathcal{R}}_x$	$R_\pi$	$\mathcal{C}$	$\mathcal{T}_{\text{ferm}}$	$R_{\pi/3}$ (isotropic limit)
$M_0 \rightarrow$	$M_0$	$M_0$	$-M_0$	$-M_0^\dagger$	$M_0^\dagger$	$-M_0$
$M_1 \rightarrow$	$e^{i\mathbf{K}_1 \cdot \delta\mathbf{r}} M_1$	$M_2$	$M_1$	$M_1^\dagger$	$M_1^\dagger$	$M_3$
$M_2 \rightarrow$	$e^{i\mathbf{K}_2 \cdot \delta\mathbf{r}} M_2$	$M_1$	$M_2$	$M_2^\dagger$	$M_2^\dagger$	$M_1$
$M_3 \rightarrow$	$e^{i\mathbf{K}_3 \cdot \delta\mathbf{r}} M_3$	$M_3$	$M_3$	$M_3^\dagger$	$M_3^\dagger$	$M_2$
$M_{R/L} \rightarrow$	$e^{\pm i\mathbf{Q} \cdot \delta\mathbf{r}} M_{R/L}$	$M_{R/L}$	$M_{L/R}$	$M_{L/R}^\dagger$	$M_{R/L}^\dagger$	$M_{L/R}$

correlations at each of the five momenta  $\mathbf{\Pi}_j$  of Fig. 7. This remarkable property stems from the enlarged global SU(4) flavor symmetry enjoyed by the AVL. For wave vectors near  $\mathbf{\Pi}_j$ , the in-plane structure factor thus scales as

$$S^{+-}(\mathbf{k} = \mathbf{\Pi}_j + \mathbf{q}, \omega) \sim A_j \frac{\Theta(\omega^2 - \mathbf{q}^2)}{(\omega^2 - \mathbf{q}^2)^{1-\eta_m/2}}. \quad (61)$$

The anomalous dimension  $\eta_m$  is given in the large- $N$  limit by

$$\eta_m \approx 0.53N - 1. \quad (62)$$

Setting  $N=4$  yields  $\eta_m \approx 1.12$  and  $\Delta_m \approx 1.04$ . While the scaling dimension is the same at each wave vector, it is important to keep in mind that the amplitudes  $A_j$  can vary significantly at different momenta. For example, near the limit of decoupled chains the amplitude at  $\mathbf{K}_3$  should be much suppressed relative to the other four wave vectors, which are near  $k_x = \pi$  where most of the activity would be expected.

We note here that while exclusion of the bare monopole  $M_0$  from a continuum expression for  $S^+$  was not obvious at the outset, this conclusion is quite reasonable physically in light of the spin correlations discussed above. If this exclusion did *not* occur, then the dynamic spin structure factor  $S^{+-}$  would exhibit the same power-law correlations at zero momentum and the five wave vectors in Fig. 7. This would be quite surprising given that one would intuitively expect subdominant correlations at zero momentum in an antiferromagnet.

The locations of the leading in-plane correlations in the AVL are suggestive of proximity to magnetically ordered phases involving condensation of  $S^+$  at the momenta shown in Fig. 7. We will explore some of these states below.

## V. PROXIMATE PHASES TO THE ALGEBRAIC VORTEX LIQUID

In this section we explore the neighboring phases of the AVL that are encoded by the effective Lagrangian (30). Response properties of the bosonic spin system will be obtained by introducing an external probing field  $A^{\text{ext}}$  that couples in the dual theory via Eq. (35). As discussed in Sec. IV A, we will assume  $\kappa=0$  so that  $A^{\text{ext}}$  couples to both the original boson currents  $\delta j = (\nabla \times a)/2\pi$  and the Chern-Simons flux. This exploration will provide some guidance as to where in the phase diagram the AVL lies, and is also useful because a study of the phase diagram within a direct Landau analysis of the spin model is hindered by Berry phases.

Descendants of the AVL are obtained by giving the fermions a mass, which destabilizes the vortex liquid leading to a

wealth of possible states. Here, we will restrict our attention to nearby states favored by the interactions  $\mathcal{L}_{4f}$ . Although we postulated above that such terms are irrelevant in the AVL critical theory, sufficiently strong four-fermion interactions are nevertheless expected to generate fermion masses and destroy the AVL. We will focus, in particular, on states arising from the generation of *enhanced* fermion mass terms, as the AVL will likely be more susceptible to realizing such states. Moreover, for simplicity we will consider the spatially isotropic limit  $J=J'$ . In this case, the four-fermion terms  $\mathcal{L}_{4f}$  can be written in terms of enhanced bilinears in Table IV as follows:

$$\begin{aligned} \mathcal{L}_{4f} = & u_1 \mathcal{M}_{KL}^2 + u_2 \mathcal{M}_{\sqrt{3} \times \sqrt{3}}^2 + u_3 \mathcal{M}_{SS}^\dagger \mathcal{M}_{SS} \\ & + \sum_{j=1}^3 (u_4 \mathcal{K}_j^2 + u_5 \mathcal{K}'_j{}^2 + u_6 \mathcal{P}_j^\dagger \mathcal{P}_j) + \mathcal{L}_{4f,ne}. \end{aligned} \quad (63)$$

The last term  $\mathcal{L}_{4f,ne}$  represents four-fermion interactions composed entirely of nonenhanced bilinears, which will not be of interest here. Though not unique, this form provides a useful organization of the four-fermion interactions based on their translation and rotation properties. Our exploration below is by no means intended to be exhaustive; rather, our aim is to illustrate some representative examples of the proximate phases that can be analyzed in the fermionized vortex theory.

### A. Kalmeyer-Laughlin spin liquid

Consider first the addition of a mass term  $m \mathcal{M}_{KL} = m \bar{\psi} \psi$ , which is favored by a large negative  $u_1$  interaction above. This mass respects all symmetries except  $\mathcal{T}_{\text{ferm}}$ , and drives the system into a  $\nu=1/2$  fractional quantum Hall state for the original bosons, which breaks *physical* time-reversal symmetry. In other words, the physical spin state obtained by the addition of  $m \mathcal{M}_{KL}$  is the Kalmeyer-Laughlin chiral spin-liquid.<sup>7,8</sup>

To demonstrate this, let us first integrate out the massive fermions. Since all flavors have the same mass  $m$  with the same sign, integrating out the fermions induces a Chern-Simons term for  $(a+A)_\mu$ . The Lagrangian is then

$$\begin{aligned} \mathcal{L}_{a,A} = & \frac{1}{2e^2} (\nabla \times a)^2 + \frac{i}{4\pi} A (\nabla \times A) + \frac{i \text{sign}(m)}{2\pi} \\ & \times (a+A) [\nabla \times (a+A)] - \frac{i}{2\pi} A^{\text{ext}} [\nabla \times (a+A)]. \end{aligned} \quad (64)$$

The spectrum for the above Lagrangian is gapped, which can

be verified by integrating out the Chern-Simons field  $A$ . Integrating out further the gauge field  $a$ , we arrive at an effective Lagrangian for the probing field  $A^{\text{ext}}$ ,

$$\mathcal{L}_{\text{eff}} = -\text{sign}(m) \frac{i\sigma_{xy}}{2} A^{\text{ext}} (\nabla \times A^{\text{ext}}), \quad (65)$$

with  $\sigma_{xy} = \nu/2\pi = 1/4\pi$ . Thus Eq. (65) characterizes the response for a  $\nu=1/2$  fractional quantum Hall state of the original bosons as claimed. We remark here that this physics results with either sign for the mass  $m$ . Had we instead chosen to couple  $A^{\text{ext}}$  only to the original boson currents [i.e., with  $\kappa=1$  in Eq. (35)], then a particular sign of the mass would have to be chosen relative to the sign of the Chern-Simons flux in order to recover the Kalmeyer-Laughlin state. Once again, we see that endowing the Chern-Simons flux with boson charge leads to response properties of the spin system that are insensitive to the direction of flux attachment as desired.

What is the nature of the gapped excitations in this phase? Consider acting on the ground state with the fermion field  $\psi^{\dagger}$ . The added fermion couples to the sum  $\tilde{a} = a + A$ . By examining the action obtained by retaining  $\tilde{a}$  and integrating out the Chern-Simons field, we see that the system dynamics binds  $\Delta \times \tilde{a} = -\pi$  flux to the fermion (which also carries  $2\pi$  Chern-Simons flux). Thus, the fermion is turned into a *semi-ionic* excitation carrying spin- $\frac{1}{2}$ . This is precisely the gapped semionic spinon in the Kalmeyer-Laughlin state.

## B. Magnetically ordered phases

The remaining states we consider arise from generating specific fermion mass terms of the form  $m\bar{\psi}\hat{W}\psi$ , where  $\hat{W}$  has two  $+1$  and two  $-1$  eigenvalues. Hence, two fermion modes have mass  $m$ , while the other two have mass  $-m$ . In all such phases, the vortices are “insulating,” and the “photon” in the dual gauge field  $a$  can freely propagate. The gapless photon is revealed upon integrating out the massive fermions, which induces only a generic Maxwell term for the field  $\tilde{a} = a + A$ . These vortex insulators correspond to magnetically ordered phases of the spin system. The gapless photon is the Goldstone spin-wave at zero-momentum arising from the broken continuous  $U(1)$  spin symmetry. Moreover, the probing field  $A^{\text{ext}}$  is massive here, which is the “Meissner effect” expected for the superfluid phase of the original bosons. Our objective below will be to disentangle the spin order that arises in different vortex insulators. As we will see, magnetically ordered states neighboring the AVL fall into two categories: conventional  $XY$  spin-ordered phases and “supersolids,” which additionally develop  $S^z$  order.

### 1. $XY$ spin-ordered states

Consider the addition of a mass term  $m\mathcal{M}_{\sqrt{3}\times\sqrt{3}}$ , which is favored by a large negative  $u_2$  in Eq. (63). Microscopically, this mass can be identified with a staggered vortex chemical potential that causes the vortices to preferentially occupy one of the two sublattices of the honeycomb. The resulting state is the vortex “charge density wave” (CDW) shown in Fig. 8(a), where the vortex density is enhanced on the filled sites and depleted on the open sites.

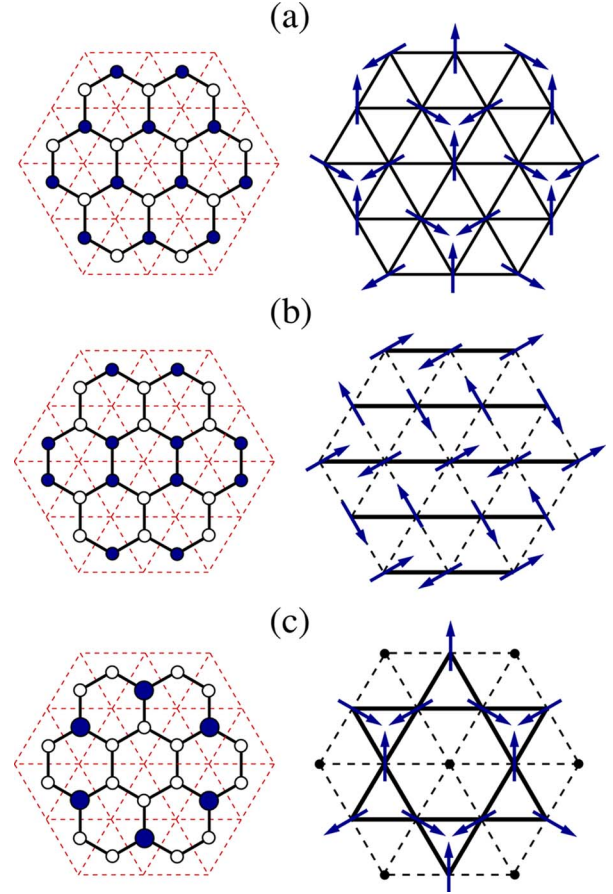


FIG. 8. (Color online) Vortex charge density waves (CDWs) proximate to the AVL in the isotropic limit  $J=J'$ , along with the corresponding spin structures. Vortices preferentially occupy filled honeycomb sites. On the right-hand side the satisfied bonds of the triangular lattice are solid, dashed lines represent less satisfied bonds, and filled circles denote sites whose spins fluctuate around zero mean.

To identify the corresponding spin structure, first recall that the leading  $S^{+-}$  spin correlations in the AVL occur at wave vectors  $\pm\mathbf{Q}$  and  $\mathbf{K}_{1,2,3}$  of Fig. 7. It is natural, then, to expect that magnetically ordered descendants of the AVL will involve condensation of  $S^+$  at these wave vectors. We will assume this is the case, and search for the symmetry equivalent of  $\mathcal{M}_{\sqrt{3}\times\sqrt{3}}$  by considering bilinears involving  $S^{\pm}$  at these wave vectors. The answer is unique (up to an overall sign), and we identify

$$\mathcal{M}_{\sqrt{3}\times\sqrt{3}} \sim S_{\mathbf{Q}}^+ S_{-\mathbf{Q}}^- - S_{-\mathbf{Q}}^+ S_{\mathbf{Q}}^-. \quad (66)$$

Since  $\langle \mathcal{M}_{\sqrt{3}\times\sqrt{3}} \rangle \neq 0$  in this vortex CDW, it follows that the spin order can be obtained from  $\langle S_{\mathbf{Q}}^+ \rangle \neq 0$ ,  $\langle S_{-\mathbf{Q}}^+ \rangle = 0$  (or vice versa, depending on the sign of the mass  $m$ ). This is the well known  $\sqrt{3} \times \sqrt{3}$  spiral state depicted in Fig. 8(a). We note that our identification in Eq. (66) holds in the anisotropic case as well; in this regime an incommensurate spiral results.

As another example, assume the  $u_4$  interaction is strong enough that a mass term  $\sum_j m_j \mathcal{K}_j$  is generated. This mass similarly corresponds to a modulated vortex chemical poten-

tial which drives CDW ordering. With only quartic fermion terms, there is a large degeneracy of possible states due to the arbitrariness in the relative values of  $m_{1,2,3}$ . This degeneracy is broken, however, by higher-order terms in the action, which select either (I)  $m_i \neq 0$ ,  $m_{j \neq i} = 0$ , or (II)  $|m_1| = |m_2| = |m_3| \neq 0$ . The resulting vortex CDW's are shown in Figs. 8(b) and 8(c), respectively.

The spin order in these states can be determined using the same logic as above. Here, we identify

$$\mathcal{K}_i \sim i \epsilon_{ijk} S_{\mathbf{K}_j}^+ S_{\mathbf{K}_k}^- \quad (67)$$

Consider case (I) first, with say  $\langle \mathcal{K}_{1,2} \rangle = 0$  and  $\langle \mathcal{K}_3 \rangle \neq 0$ . Equation (67) then implies that  $\langle S_{\mathbf{K}_3}^+ \rangle = 0$  and  $\langle S_{\mathbf{K}_{1,2}}^+ \rangle \sim e^{i\varphi_{1,2}}$ , which yields  $\langle \mathcal{K}_3 \rangle \sim \sin(\varphi_1 - \varphi_2)$ . To maximize  $|\langle \mathcal{K}_3 \rangle|$ , which is energetically favored by the large  $u_4$  interaction, the phases  $\varphi_1$  and  $\varphi_2$  are chosen to differ by  $\pi/2$ . The resulting spin order is shown on the right-hand side of Fig. 8(b). Now let us consider case (II), where  $|\langle \mathcal{K}_1 \rangle| = |\langle \mathcal{K}_2 \rangle| = |\langle \mathcal{K}_3 \rangle| \neq 0$ . Here we take  $\langle S_{\mathbf{K}_j}^+ \rangle \sim e^{i\varphi_j}$ , yielding  $\langle \mathcal{K}_1 \rangle \sim \sin(\varphi_2 - \varphi_3)$ , etc. In this case the phases  $\varphi_{1,2,3}$  must differ by either  $\pi/3$  or  $2\pi/3$ , which leads to the spin order illustrated in Fig. 8(c). On the right-hand side of Fig. 8, the solid lines indicate satisfied bonds, while the filled circles denote triangular lattice sites with spins fluctuating around zero mean.

A similar analysis can be used to identify the states arising from spontaneously generated mass involving the enhanced bilinears  $\mathcal{P}_j$ . Such mass terms give rise to modulated nearest-neighbor hopping amplitudes for the vortices, and drive vortex ‘‘valence bond solid’’ (VBS) order. Since  $\mathcal{P}_j$  carries momentum  $\mathbf{K}_j + \mathbf{Q}$ , the spin structures corresponding to these VBS phases involve condensation of both  $S_{\mathbf{Q}}^+$  and  $S_{\mathbf{K}_j}^+$ . At present it is unclear what order is driven by  $\mathcal{K}_j^+$  mass terms, due to the fact that they arise from second-neighbor vortex hopping, which does not have a clear interpretation for the spin system.

## 2. Supersolids

Finally, consider a mass term  $m(e^{i\gamma} M_{SS}^\dagger + \text{H.c.})$  generated by a large  $u_3$  interaction. Microscopically, this mass induces both modulations in the nearest-neighbor vortex hopping amplitudes and modulations in the gauge flux piercing the honeycomb plaquettes. The degeneracy in the phase  $\gamma$  is lifted by higher-order terms in the action, which select either  $\gamma = n\pi/3$  or  $\gamma = (2n+1)\pi/6$ , where  $n$  is an integer. The vortex states for these two cases are shown in Figs. 9(a) and 9(b), respectively. In the figure, the direction of induced flux through a given plaquette is indicated with a  $\pm$  sign, and the bold honeycomb links have the dominant hopping amplitudes. In Fig. 9(a), the induced flux is twice as large on ‘‘+’’ plaquettes; in (b), the induced flux is equal and opposite on ‘‘ $\pm$ ’’ plaquettes and vanishes on others.

These lattice-scale gauge flux modulations signify the onset of  $S^z$  ordering in the spin system,

$$\langle S^z \rangle \sim \cos(\mathbf{Q} \cdot \mathbf{r} + \gamma). \quad (68)$$

Since there is a gapless photon in these states, the continuous U(1) spin symmetry is also broken. Hence the in-plane spin

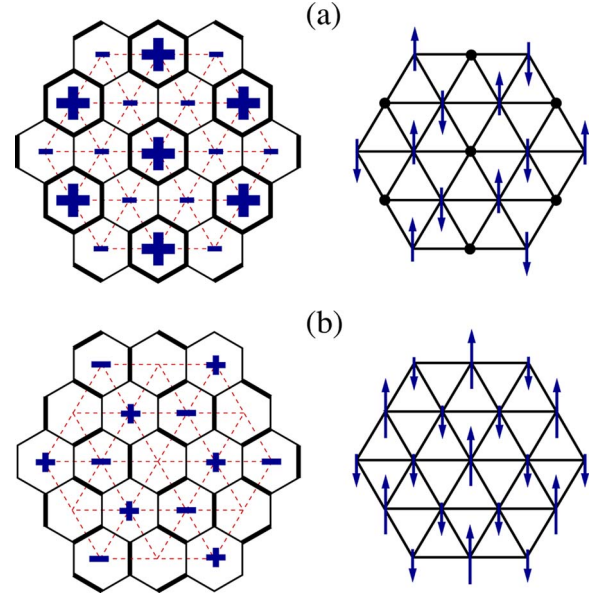


FIG. 9. (Color online) Supersolids neighboring the AVL. On the left-hand side, the direction of induced gauge flux is specified by a  $\pm$  sign, and the hopping amplitudes are dominant along bold links of the honeycomb. The ‘‘solid’’ ordering pattern for  $\langle S^z \rangle$  follows the pattern of induced gauge flux, while the ‘‘superfluid’’ order for  $\langle S^+ \rangle$  is shown on the right-hand side. Filled circles denote sites with  $\langle S^+ \rangle = 0$ . The overall spin structure can be viewed as a spiral state, tilted into the  $(S^y, S^z)$  plane.

components order as well, so that these states are examples of ‘‘supersolids.’’ Using the symmetry of the vortex phases and the uncertainty principle as a guide, the simplest assumption for the  $S^+$  order is shown on the right-hand side of Figs. 9(a) and 9(b). The filled circles in the figure denote sites with  $\langle S^+ \rangle = 0$ . The in-plane and out-of-plane spin structure can be collectively viewed as a coplanar spiral state rotated into, for instance, the  $(S^y, S^z)$  plane. Both spin patterns exhibit a  $\sqrt{3} \times \sqrt{3}$  periodicity. The difference is that in Fig. 9(a) spins on one sublattice point along the hard  $S^z$  axis, while in Fig. 9(b) spins on one sublattice point along the  $S^y$  axis.

## VI. DISCUSSION

In this paper we have performed a detailed characterization of a ‘‘critical’’ spin liquid, the algebraic vortex liquid, which arises rather naturally out of a reformulation of the easy-plane spin model in terms of fermionized vortex degrees of freedom. Among the most striking predictions for the AVL is the behavior of the dynamical spin correlations. As a consequence of an emergent global SU(4) symmetry, the in-plane spin structure factor  $S^{+-}$  exhibits enhanced power-law correlations with *identical* exponents at the five inequivalent momenta shown in Fig. 7. Due to the easy-plane character of the AVL, the out-of-plane spin correlations behave quite differently. The  $S^{zz}$  structure factor exhibits enhanced power-law correlations only at the spiral ordering wave vectors ( $\pm \mathbf{Q}$  in Fig. 7), and is generally expected to be weaker than  $S^{+-}$ . These nontrivial features in the spin struc-

ture factor distinguish the AVL from other known spin liquids, and should serve as useful characterizations for identifying this phase experimentally.

Our study was partly motivated by the spin- $\frac{1}{2}$  triangular antiferromagnet  $\text{Cs}_2\text{CuCl}_4$ , whose spin dynamics have been explored with neutron scattering.<sup>4,5</sup> Although this material develops long range spiral order at low temperatures  $T \lesssim T_N = 0.62$  K, the dynamical structure factor exhibits anomalous power laws at intermediate energies, both in the ordered phase and in a range of temperatures above  $T_N$ . Such power-law behavior is reminiscent of spin-liquid physics, and several scenarios for its origin have been proposed. These include physics dominated by one-dimensional chains,<sup>43,44</sup> a two-dimensional algebraic spin liquid,<sup>13</sup> the  $Z_2$  spin liquid,<sup>45,46</sup> and a quantum critical point scenario,<sup>47</sup> as well as more conventional explanations such as nonlinear spin-wave theory.<sup>48</sup>

Possible application of the AVL to  $\text{Cs}_2\text{CuCl}_4$  has been discussed in some detail in Ref. 26. The most intriguing observation here is that the dynamical structure factor was found experimentally to decay with the same power-law near wave vectors  $\mathbf{K}_{1,2}$  and  $\mathbf{Q}$  in Fig. 7,<sup>5</sup> consistent with our expectations for the AVL. It is important to keep in mind, however, that the dual vortex formulation employed here requires an easy-plane  $U(1)$  spin symmetry so that vortices exist as stable topological excitations. This imparts the AVL with a distinct easy-plane character, unlike other theoretical proposals which retain full  $SU(2)$  spin symmetry. Although there is a microscopic easy-plane spin anisotropy in  $\text{Cs}_2\text{CuCl}_4$  due to a Dzyaloshinskii-Moriya interaction, this coupling is fairly weak, and it is therefore not clear whether the AVL described here can be applied directly (some scenarios are considered in Ref. 26). An interesting possibility is that the AVL has an  $SU(2)$ -invariant relative which may be relevant for  $\text{Cs}_2\text{CuCl}_4$ , though we do not know how to access such a state theoretically. One speculation in this respect is that there may exist a slave-particle description of the AVL. In particular, the direct slave-fermion approach often yields critical states dubbed algebraic spin liquids (ASLs); such states on the triangular lattice were explored in Ref. 13. The algebraic vortex liquid is not formulated using spinon fields, but predicts critical power-law spin correlations reminiscent of those in ASLs. It should also be said that spinons are strongly interacting in the ASL and cannot be thought of as free fields in any sense, and the same is true about vortices in the AVL. Unfortunately, so far we have been unable to find a spin-liquid state on the triangular lattice that would reproduce all the dominant wave vectors present in the AVL phase, but such a connection between these very different theoretical perspectives remains a tantalizing possibility.

#### ACKNOWLEDGMENTS

The authors would like to acknowledge Leon Balents and T. Senthil for many illuminating discussions, and especially Mike Hermele for an initial collaboration. This work was supported by the National Science Foundation (J. A.) through Grant Nos. PHY-9907949 (O. I. M. and M. P. A. F.) and DMR-0529399 (M. P. A. F.).

#### APPENDIX: TRANSFORMATION PROPERTIES OF THE NEGATIVE-ENERGY DIRAC SEA

This appendix is devoted to obtaining the transformation properties of  $|DS, q\rangle\langle 0|$ , which are needed for determining the quantum numbers carried by the monopole operators in QED3. Here  $|DS, q\rangle$  is the filled negative-energy Dirac sea with a  $2\pi q$  flux insertion, where  $q = \pm 1$ , and  $|0\rangle$  is the ground state with no added flux. We attack the problem in two stages. First, we constrain the transformation properties as much as possible using various general relations among symmetries. The ambiguities that still remain here are then fixed using numerical studies of monopole insertions.

#### General arguments

*Fermionic time reversal and particle-hole symmetry:* By examining Table II, we see that the flux changes sign under both  $\mathcal{T}_{\text{ferm}}$  and  $\mathcal{C}$ . Hence  $\mathcal{T}_{\text{ferm}}$  transforms the filled negative-energy Dirac sea with  $q = +1$  into the negative-energy Dirac sea with  $q = -1$ , while  $\mathcal{C}$  additionally fills the four zero modes since  $|DS, q\rangle$  is not half-filled. The ground state  $|0\rangle$ , on the other hand, is an eigenstate of both symmetries. Using  $\mathcal{T}_{\text{ferm}}^2 = \mathcal{C}^2 = 1$ , we can then define the phases of  $|DS, q\rangle$  such that

$$\mathcal{T}_{\text{ferm}}: |DS, q\rangle\langle 0| \rightarrow |DS, -q\rangle\langle 0|, \quad (\text{A1})$$

$$\mathcal{C}: |DS, q\rangle\langle 0| \rightarrow \prod_{Aa} f_{Aa, -q}^\dagger |DS, -q\rangle\langle 0|. \quad (\text{A2})$$

Both  $|DS, q\rangle$  and  $|0\rangle$  are expected to be eigenstates under the remaining symmetries in Table V, all of which leave the flux invariant. Quite generally, we then have

$$R_\pi: |DS, q\rangle\langle 0| \rightarrow e^{i\theta_\pi^q} |DS, q\rangle\langle 0|,$$

$$\tilde{\mathcal{R}}_x: |DS, q\rangle\langle 0| \rightarrow e^{i\theta_x^q} |DS, q\rangle\langle 0|,$$

$$T_{1,2}: |DS, q\rangle\langle 0| \rightarrow e^{i\theta_{1,2}^q} |DS, q\rangle\langle 0|,$$

$$R_{\pi/3}: |DS, q\rangle\langle 0| \rightarrow e^{i\theta_{\pi/3}^q} |DS, q\rangle\langle 0|, \quad (\text{A3})$$

where the last line holds only in the isotropic limit. We will now examine the general constraints on the above eigenvalues.

*Inversion:* First, one can show that the phases  $\theta_\pi^q$  must be independent of  $q$  by using the commutation relation  $[R_\pi, \mathcal{T}_{\text{ferm}}] = 0$  when acting on *half-filled* states, which are gauge invariant. For example, it follows from  $[R_\pi, \mathcal{T}_{\text{ferm}}] F_{0,q}^\dagger |DS, q\rangle = 0$  that  $\theta_\pi^q = \theta_\pi^{-q}$ . Furthermore,  $R_\pi^2 = 1$  implies that  $e^{i\theta_\pi^q} \equiv \zeta_\pi = \pm 1$ , so we have

$$R_\pi: |DS, q\rangle\langle 0| \rightarrow \zeta_\pi |DS, q\rangle\langle 0|. \quad (\text{A4})$$

The sign  $\zeta_\pi$  is in principle fixed, but cannot be determined using general relations alone.

*Modified reflection:* Similarly, it follows from the commutation relations  $[\tilde{\mathcal{R}}_x, \mathcal{C}] = [\tilde{\mathcal{R}}_x, \mathcal{T}_{\text{ferm}}] = 0$  (on physical states) that

$$\tilde{\mathcal{R}}_x: |DS, q\rangle\langle 0| \rightarrow i\zeta_x |DS, q\rangle\langle 0|. \quad (\text{A5})$$

The sign  $\zeta_x = \pm 1$  is also fixed, but cannot be determined from this general analysis.

*Translations:* We constrain the phases  $\theta_{1,2}^f$  by first assuming the following operator relations hold when acting on gauge-invariant states:

$$T_2 R_\pi = R_\pi T_2^{-1}, \quad (\text{A6})$$

$$T_2 \tilde{\mathcal{R}}_x = \tilde{\mathcal{R}}_x T_1 T_2, \quad (\text{A7})$$

since the left-hand and right-hand sides transform the lattice identically. The first relation implies  $e^{i\theta_2^f} = \pm 1$ , while using the second we conclude  $e^{i\theta_1^f} = -1$ . We can fix the former sign by now specializing to the isotropic limit. Here, we have an additional symmetry relation,

$$T_1 R_{\pi/3} = R_{\pi/3} T_2^{-1}, \quad (\text{A8})$$

that holds when acting on physical states. From this we obtain  $e^{i\theta_1^f} = e^{i\theta_2^f} = -1$  in the isotropic limit. By continuity, we assume this carries over in the anisotropic limit as well so that

$$T_{1,2}: |DS, q\rangle\langle 0| \rightarrow -|DS, q\rangle\langle 0|. \quad (\text{A9})$$

*Rotations (isotropic limit):* The commutation relation  $[R_{\pi/3}, T_{\text{ferm}}] = 0$  on physical states implies that  $e^{i\theta_{\pi/3}^q} = e^{-i\theta_{\pi/3}^q}$ . Moreover, the relation  $R_{\pi/3}^3 = R_\pi$  together with commutation with particle-hole symmetry yields  $e^{i\theta_{\pi/3}^q} = \zeta_\pi e^{2iq\pi/3}$ . Thus, we have

$$R_{\pi/3}: |DS, q\rangle\langle 0| \rightarrow \zeta_\pi e^{2iq\pi/3} |DS, q\rangle\langle 0|. \quad (\text{A10})$$

We have now arrived at the transformation properties listed in Eq. (59). As discussed in Sec. IV C 2, determining the ambiguities in  $\zeta_\pi$  and  $\zeta_x$  that arose above is crucial for understanding the in-plane spin correlations in the AVL. We will attempt to sort out these uncertainties by appealing to numerics, discussed below.

### Numerical diagonalization

For convenience, we specialize to the isotropic limit  $J = J'$  for the remainder of this appendix. Consider the mean-field Hamiltonian (16) generalized to include arbitrary flux insertions,

$$\mathcal{H}_{\text{MF}} = -t \sum_{\langle \mathbf{x}\mathbf{x}' \rangle} (d_{\mathbf{x}}^\dagger d_{\mathbf{x}'} e^{-i(a_{\mathbf{x}\mathbf{x}'}^0 + \delta a_{\mathbf{x}\mathbf{x}'})} + \text{H.c.}). \quad (\text{A11})$$

Here  $a^0$  is the gauge field giving rise to a background  $\pi$  flux as before, while  $\delta a$  gives rise to any added flux. We have numerically diagonalized the above Hamiltonian on finite systems to obtain the spectrum of single-particle energies and wave functions. Specifically, we considered lattices composed of  $N_{\text{rings}}$  concentric “rings” of honeycomb sites. For example, Figs. 8 and 9 illustrate systems with  $N_{\text{rings}} = 2$  and 3, respectively. System sizes up to  $N_{\text{rings}} = 17$ , consisting of 1734 lattice sites, were studied. Flux insertions varying from

0 to  $2\pi$  were taken to be uniformly spread within the first several innermost rings. A variety of boundary conditions were used, namely, open boundary conditions; “Klein bottle” boundary conditions, where one connects boundary sites with coordination number 2 and their inversion counterparts; and modifications of the latter, where one connects only a subset of such boundary sites and their inversions. (Note that open boundary conditions are problematic when  $N_{\text{rings}}$  is odd, because with no added flux there are two degenerate zero-energy modes and therefore no unique ground state  $|0\rangle$ .) Other boundary conditions mentioned above give a unique ground state as desired.) Such geometries break translational invariance, but are particularly convenient for addressing the symmetries of interest here.

With the single-particle wave functions in hand, one can explicitly construct the states  $|0\rangle$  and  $|DS, +1\rangle$ . The ground state  $|0\rangle$  is simply built from all negative-energy wave functions. More care must be taken, however, in constructing  $|DS, +1\rangle$ . In a finite system, the four quasilocalized “zero modes”—which are excluded from this state—are split away from zero energy, two above zero and two below. Identifying these quasilocalized modes is essential, particularly since the boundaries can introduce additional “edge” modes near zero energy. These modes can be distinguished by the behavior of their wave functions. Most of the probability weight lies near the flux insertion for the quasilocalized modes, whereas the dominant weight for the edge modes occurs near the boundary. A useful diagnostic for this comparison is the “ring participation”  $P_n(\phi)$ , which for a particular wave function  $\phi$  gives the probability weight summed over honeycomb ring  $n$ , normalized by the number of sites in the ring. More explicitly,

$$P_n(\phi) = \frac{1}{N_{\text{sites}}(n)} \sum_{i \in n} |\phi(i)|^2, \quad (\text{A12})$$

where  $N_{\text{sites}}(n)$  is the total number of sites in ring  $n$  and  $i$  is summed over all sites in the ring. Figure 10 displays the ring participation for the first several wave functions above zero energy in a system with  $N_{\text{rings}} = 14$ , open boundary conditions, and  $2\pi$  flux inserted within the first four innermost rings. This illustrates the clear difference between the quasilocalized modes (solid lines) and other low-energy states (dashed lines). In most cases observed this distinction allows one to identify the former, which are the modes of interest. Once these have been located, the state  $|DS, +1\rangle$  can be built out of the remaining negative-energy wave functions.

The inversion eigenvalues for  $|0\rangle$  and  $|DS, +1\rangle$  are then simply given by the product of inversion eigenvalues for the single-particle wave functions contributing to these states. We find that the parity under inversion for  $|0\rangle$  and  $|DS, +1\rangle$  depends on both the system size and boundary conditions. However, in all cases where the quasilocalized modes can be clearly resolved, the *product* of the inversion eigenvalues of  $|0\rangle$  and  $|DS, +1\rangle$ —which gives the sign  $\zeta_R$ —is geometry independent. In particular, we find  $\zeta_R = -1$ .

Some insight into this result can be obtained by viewing the  $2\pi$  flux as being inserted adiabatically. Numerically, this

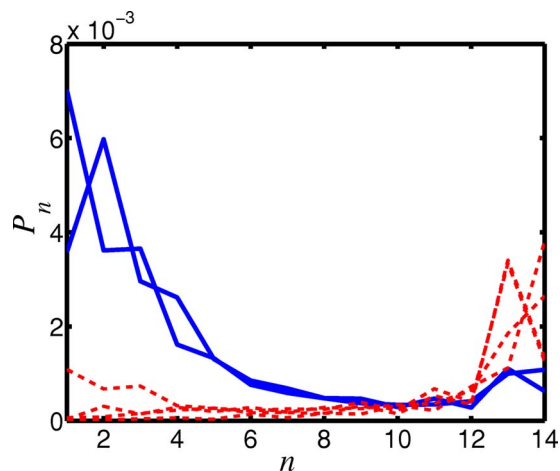


FIG. 10. (Color online) Ring participation  $P_n$  versus the ring index  $n$  for the first several wave functions above zero energy. The data correspond to a system with  $N_{\text{rings}}=14$ , open boundary conditions, and a  $2\pi$  flux insertion spread within the first four innermost rings. The quasilocalized modes (solid curves), whose wave functions are peaked near the flux insertion, are clearly distinguishable from other low-energy modes (dashed lines).

is achieved by ramping the added flux from 0 to  $2\pi$  in several stages and monitoring the evolution of the energy levels during the insertion. In all cases studied, no levels cross zero energy during the evolution (though we do not have an ar-

gument for why this is the case). This implies that the quantum numbers for the state with all negative-energy modes occupied are unchanged by the  $2\pi$  flux insertion. Moreover, we observe that the two quasilocalized modes with energy slightly below zero always have *opposite* inversion eigenvalues. Consequently, the states  $|0\rangle$  and  $|DS, +1\rangle$  must also have opposite inversion parity. Why the quasilocalized modes split in this way is unclear at the moment, but would be useful to explore.

Obtaining the sign  $\zeta_x$  from numerics is more subtle due to the antiunitarity of  $\tilde{\mathcal{R}}_x$ . A more useful symmetry to examine is the unitary operation  $\mathcal{R}'_x = \tilde{\mathcal{R}}_x C T_{\text{ferm}}$ , which has eigenvalues  $\pm 1$ . We will use the eigenvalues of  $\mathcal{R}'_x$  to back out the sign  $\zeta_x$ . The fact that we find no zero-energy level crossings provides a useful shortcut to this end (but is not necessary). Again, the quantum numbers of the state with all negative-energy modes filled are then conserved under a  $2\pi$  flux insertion. In particular, the ground state  $|0\rangle$  and the  $q=1$  Dirac sea with the two negative-energy quasilocalized modes filled must have identical eigenvalues under both  $\mathcal{R}'_x$  and  $R_{\pi/3}$ . There are just two candidates for the latter state, since only  $(F_{R,+1}^\dagger - F_{L,+1}^\dagger)|DS, +1\rangle$  and  $(F_{1,+1}^\dagger + F_{2,+1}^\dagger + F_{3,+1}^\dagger)|DS, +1\rangle$  have the same rotation eigenvalue as the ground state  $|0\rangle$ . Furthermore, under  $\mathcal{R}'_x$  both candidates have eigenvalues that differ from  $|0\rangle$  by  $-\zeta_x$ . Hence in either case we conclude that  $\zeta_x = -1$ .

- <sup>1</sup>P. W. Anderson, Mater. Res. Bull. **8**, 153 (1973).
- <sup>2</sup>R. R. P. Singh and D. A. Huse, Phys. Rev. Lett. **68**, 1766 (1992).
- <sup>3</sup>L. Capriotti, A. E. Trumper, and S. Sorella, Phys. Rev. Lett. **82**, 3899 (1999).
- <sup>4</sup>R. Coldea, D. A. Tennant, A. M. Tsvetlik, and Z. Tylczynski, Phys. Rev. Lett. **86**, 1335 (2001).
- <sup>5</sup>R. Coldea, D. A. Tennant, and Z. Tylczynski, Phys. Rev. B **68**, 134424 (2003).
- <sup>6</sup>R. Coldea, D. A. Tennant, K. Habicht, P. Smeibidl, C. Wolters, and Z. Tylczynski, Phys. Rev. Lett. **88**, 137203 (2002).
- <sup>7</sup>V. Kalmeyer and R. B. Laughlin, Phys. Rev. Lett. **59**, 2095 (1987).
- <sup>8</sup>V. Kalmeyer and R. B. Laughlin, Phys. Rev. B **39**, 11879 (1989).
- <sup>9</sup>K. Yang, L. K. Warman, and S. M. Girvin, Phys. Rev. Lett. **70**, 2641 (1993).
- <sup>10</sup>E. Fradkin, Phys. Rev. Lett. **63**, 322 (1989).
- <sup>11</sup>S. Sachdev, Phys. Rev. B **45**, 12377 (1992).
- <sup>12</sup>R. Moessner and S. L. Sondhi, Phys. Rev. Lett. **86**, 1881 (2001).
- <sup>13</sup>Y. Zhou and X. G. Wen, cond-mat/0210662 (unpublished).
- <sup>14</sup>N. Read and S. Sachdev, Phys. Rev. Lett. **62**, 1694 (1989).
- <sup>15</sup>S. Sachdev and K. Park, Ann. Phys. (N.Y.) **298**, 58 (2002).
- <sup>16</sup>C. Lannert, M. P. A. Fisher, and T. Senthil, Phys. Rev. B **63**, 134510 (2001).
- <sup>17</sup>T. Senthil, L. Balents, S. Sachdev, A. Vishwanath, and M. P. A. Fisher, Phys. Rev. B **70**, 144407 (2004).
- <sup>18</sup>T. Senthil and M. P. A. Fisher, Phys. Rev. B **62**, 7850 (2000).
- <sup>19</sup>M. P. A. Fisher and D. H. Lee, Phys. Rev. B **39**, 2756 (1989).
- <sup>20</sup>Z. Tesanovic, Phys. Rev. Lett. **93**, 217004 (2004).
- <sup>21</sup>A. Melikyan and Z. Tesanovic, Phys. Rev. B **71**, 214511 (2005).
- <sup>22</sup>L. Balents, L. Bartosch, A. Burkov, S. Sachdev, and K. Sengupta, Phys. Rev. B **71**, 144508 (2005).
- <sup>23</sup>L. Balents, L. Bartosch, A. Burkov, S. Sachdev, and K. Sengupta, Phys. Rev. B **71**, 144509 (2005).
- <sup>24</sup>A. A. Burkov and L. Balents, Phys. Rev. B **72**, 134502 (2005).
- <sup>25</sup>J. Alicea, O. I. Motrunich, M. Hermele, and M. P. A. Fisher, Phys. Rev. B **72**, 064407 (2005).
- <sup>26</sup>J. Alicea, O. I. Motrunich, and M. P. A. Fisher, Phys. Rev. Lett. **95**, 247203 (2005).
- <sup>27</sup>W. Zheng, J. O. Fjærestad, R. R. P. Singh, R. H. McKenzie, and R. Coldea, Phys. Rev. Lett. **96**, 057201 (2006).
- <sup>28</sup>R. G. Melko, A. Paramekanti, A. A. Burkov, A. Vishwanath, D. N. Sheng, and L. Balents, Phys. Rev. Lett. **95**, 127207 (2005).
- <sup>29</sup>D. Heidarian and K. Damle, Phys. Rev. Lett. **95**, 127206 (2005).
- <sup>30</sup>S. Wessel and M. Troyer, Phys. Rev. Lett. **95**, 127205 (2005).
- <sup>31</sup>M. Boninsegni and N. Prokof'ev, Phys. Rev. Lett. **95**, 237204 (2005).
- <sup>32</sup>Weihong Zheng, R. H. McKenzie, and R. R. Singh, Phys. Rev. B **59**, 14367 (1999).
- <sup>33</sup>T. W. Appelquist, M. Bowick, D. Karabali, and L. C. R. Wijewardhana, Phys. Rev. D **33**, 3704 (1986).
- <sup>34</sup>W. Rantner and X.-G. Wen, Phys. Rev. B **66**, 144501 (2002).
- <sup>35</sup>M. Franz, Z. Tesanovic, and O. Vafek, Phys. Rev. B **66**, 054535 (2002).
- <sup>36</sup>M. Franz, T. Pereg-Barnea, D. E. Sheehy, and Z. Tesanovic, Phys.

- Rev. B **68**, 024508 (2003).
- <sup>37</sup>K. Kaveh and I. F. Herbut, Phys. Rev. B **71**, 184519 (2005).
- <sup>38</sup>M. Hermele, T. Senthil, and M. P. A. Fisher, Phys. Rev. B **72**, 104404 (2005).
- <sup>39</sup>S. J. Hands, J. B. Kogut, and C. G. Strouthos, Nucl. Phys. B **645**, 321 (2002).
- <sup>40</sup>S. J. Hands, J. B. Kogut, L. Scorzato, and C. G. Strouthos, Phys. Rev. B **70**, 104501 (2004).
- <sup>41</sup>R. Jackiw, Phys. Rev. D **29**, 2375 (1984).
- <sup>42</sup>V. Borokhov, A. Kapustin, and X. Wu, J. High Energy Phys. **11**, 049 (2002).
- <sup>43</sup>M. Bocquet, F. H. L. Essler, A. M. Tsvelik, and A. O. Gogolin, Phys. Rev. B **64**, 094425 (2001).
- <sup>44</sup>O. A. Starykh and L. Balents (unpublished).
- <sup>45</sup>C. H. Chung, J. B. Marston, and R. H. McKenzie, J. Phys.: Condens. Matter **13**, 5159 (2001).
- <sup>46</sup>C. H. Chung, K. Voelker, and Y. B. Kim, Phys. Rev. B **68**, 094412 (2003).
- <sup>47</sup>S. V. Isakov, T. Senthil, and Y. B. Kim, Phys. Rev. B **72**, 174417 (2005).
- <sup>48</sup>M. Y. Veillette, A. J. A. James, and F. H. L. Essler, Phys. Rev. B **72**, 134429 (2005).